THE JOURNAL OF PHYSICAL CHEMISTRY B
A JOURNAL OF THE AMERICAN CHEMICAL SOCIETY

pubs.acs.org/JPCB

Article

Singlet O_2 Oxidation of the Radical Cation versus the Dehydrogenated Neutral Radical of 9-Methylguanine in a Watson–Crick Base Pair. Consequences of Structural Context

May Myat Moe, Toru Saito, Midas Tsai, and Jianbo Liu*

Cite This: *J. Phys. Chem. B* 2022, 126, 5458–5472

Read Online

ACCESS | Metrics & More | Article Recommendations | Supporting Information

ABSTRACT: In DNA, guanine is the most susceptible to oxidative damage by exogenously and endogenously produced electronically excited singlet oxygen ($^1O_2$). The reaction mechanism and the product outcome strongly depend on the nucleobase ionization state and structural context. Previously, exposure of a monomeric 9-methylguanine radical cation ($9MG^{\bullet+}$, a model guanosine compound) to $^1O_2$ was found to result in the formation of an 8-peroxide as the initial product. The present work explores the $^1O_2$ oxidation of $9MG^{\bullet+}$ and its dehydrogenated neutral form $[9MG - H]^{\bullet}$ within a Watson–Crick base pair consisting of one-electron-oxidized 9-methylguanine–1-methylcytosine $[9MG{\cdot}1MC]^{\bullet+}$. Emphasis is placed on entangling the base pair structural context and intra-base pair proton transfer with and consequences thereof on the singlet oxygenation of guanine radical species. Electrospray ionization coupled with guided-ion beam tandem mass spectrometry was used to study the formation and reaction of guanine radical species in the gas phase. The $^1O_2$ oxidation of both $9MG^{\bullet+}$ and $[9MG - H]^{\bullet}$ is exothermic and proceeds barrierlessly either in an isolated monomer or within a base pair. Single- and multi-referential theories were tested for treating spin contaminations and multi-configurations occurring in radical–$^1O_2$ interactions, and reaction potential energy surfaces were mapped out to support experimental findings. The work provides a comprehensive profile for the singlet oxygenation of guanine radicals in different charge states and in the absence and the presence of base pairing. All results point to an 8-peroxide as the major oxidation product in the experiment, and the oxidation becomes slightly more favorable in a neutral radical form. On the basis of a variety of reaction pathways and product profiles observed in the present and previous studies, the interplay between guanine structure, base pairing, and singlet oxygenation and its biological implications are discussed.

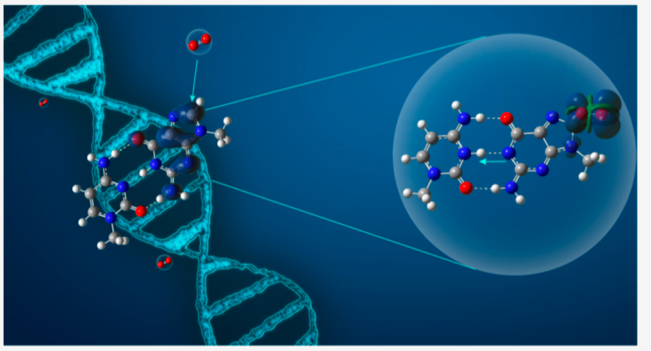

1. INTRODUCTION

Guanine represents a dominant target for one-electron oxidation and ionization due to its lowest oxidation potential ($E°$) and ionization potential (IP) within DNA components. The $E°$ versus NHE for DNA nucleosides are in the order of 1.29 V for guanosine <1.42 V for adenosine <1.6 V for deoxycytidine <1.7 V for thymidine.[1,2] The adiabatic IPs for the corresponding nucleobases[3−5] and other DNA building blocks[6,7] are in the order of 7.75 eV for guanine <8.27 eV for adenine <8.66 eV for cytosine <8.82 eV for thymine <8.9–9.5 eV (HPO_4^{2-} and $H_2PO_4^-$) <9.4–9.7 eV for deoxyribose in the gas phase, and these are lowered to 4.42 eV for guanine <4.81 eV for adenine <4.91 eV for cytosine <5.05 eV for thymine by water solvation and stabilization in aqueous solutions.[8,9] Complementary base pairing with cytosine in double-stranded DNA further decreases guanine $E°$ by 0.28–0.34 V[10,11] and IP by 0.75–0.78 eV.[12,13] As a result, the formation of the guanine radical cation ($G^{\bullet+}$) is facile upon photoionization,[5,14] ionizing radiation,[15,16] chemical oxidation,[17] electron transfer between metal complexes bound to DNA,[18] electrocatalytic oxidation,[19] type I photooxidation,[20] and so forth. Electron holes that are created by oxidation of other nucleobases may also migrate from the locus of formation to guanine sites.[21] All of these render the formation of $G^{\bullet+}$ an ultimate trap for oxidative damage to DNA.[16]

Neutral guanine is a weak base with a pK_a of 9.4 for N1; nevertheless, $G^{\bullet+}$ becomes acidic with a p*K*a of 3.9.[15] An isolated $G^{\bullet+}$ or that within single-stranded DNA would lose its N1-proton to water and form a dehydrogenated neutral radical $[G - H]^{\bullet}$ within 56 ns.[22,23] This scenario, however, changes in double-stranded DNA wherein $G^{\bullet+}$ is retained by sharing its N1-proton with the N3′ (pK_a 4.3)[24] of cytosine (C) within a

Received: May 31, 2022
Revised: June 25, 2022
Published: July 18, 2022

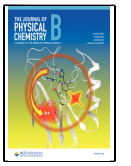

https://doi.org/10.1021/acs.jpcb.2c03748
J. Phys. Chem. B 2022, 126, 5458–5472

Scheme 1. Intra-Base Pair PT of $9MG^{\bullet+}\cdot 1MC \rightleftharpoons [9MG - H_{N1}]^{\bullet}\cdot[1MC + H_{N3'}]^{+}$, with Spin Density Contour Plots (Top) and ESP Maps (Bottom) Generated at ωB97XD/6-31+G(d,p)

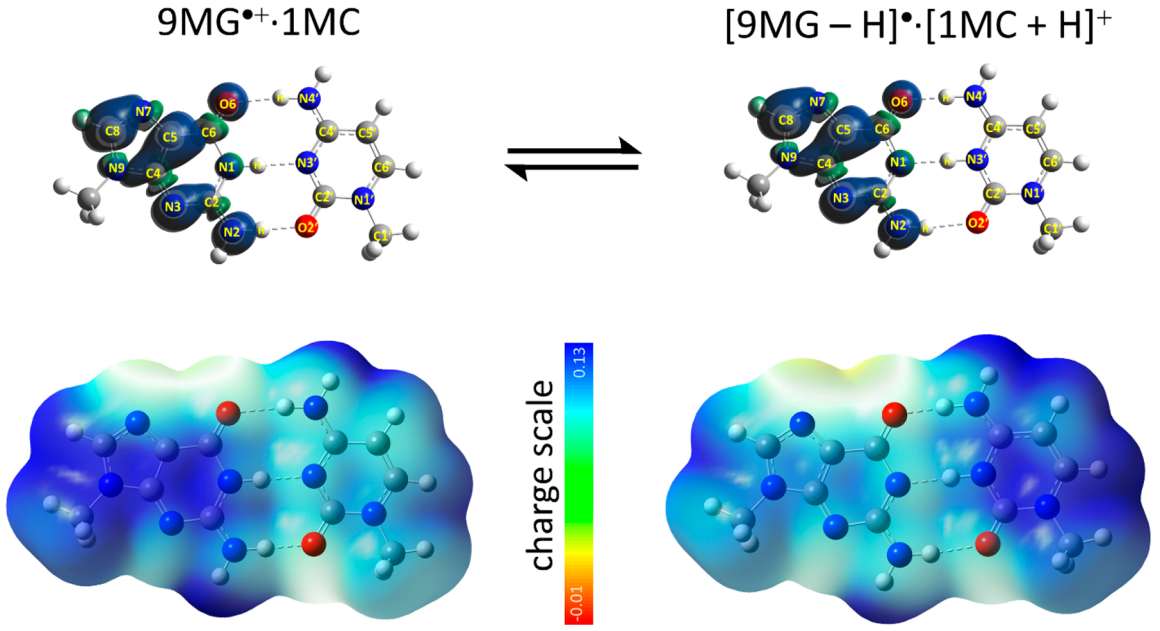

Watson−Crick base pair.[12,23,25−28] Scheme 1 illustrates intra-base pair proton transfer (PT) in a model system, 9-methylguanine−1-methylcytosine radical cation ($[9MG\cdot 1MC]^{\bullet+}$), of which the methylation at guanine N9 and cytosine N1′ mimics ribose in nucleosides. Spin density and electrostatic potential (ESP) maps in the scheme provide a graphical display of spin and charge distributions and how they are influenced by PT. PT dynamics in $[9MG\cdot 1MC]^{\bullet+}$ was recently examined in our laboratory on the basis of collision-induced dissociation (CID) tandem mass spectrometry augmented by density functional theory (DFT) and coupled-cluster theory calculations.[28] The experiment verified the coexistence of conventional $9MG^{\bullet+}\cdot 1MC$ (population 87%) and its proton-transferred counterpart $[9MG - H_{N1}]^{\bullet}\cdot[1MC + H_{N3'}]^{+}$ (population 13%) in the gas phase, and the two structures had similar dissociation energies. However, an intriguing observation is that the base pair dissociation is nonstatistical. CID product ions were overwhelmingly dominated by the fragments generated from a PT structure, that is, $[9MG - H_{N1}]^{\bullet}\cdot[1MC + H_{N3'}]^{+} \rightarrow [9MG - H]^{\bullet} + [1MC + H]^{+} \gg 9MG^{\bullet+}\cdot 1MC \rightarrow 9MG^{\bullet+} + 1MC$, which is contrary to what would happen in a statistical reaction framework. This indicates that, in an excited/activated base pair, intra-base pair PT forms dehydrogenated neutral guanine radicals and thereof prompts the biological significance of this species.

Intra-base pair PT not only leads to rare tautomer and spontaneous point mutation[29,30] but also affects DNA oxidatively generated damage. Illustrative of the latter are the different post-ionization conversions of $G^{\bullet+}$ versus $[G - H]^{\bullet}$. Transformation of $G^{\bullet+}$ begins with C8-water addition,[31] leading to the formation of a C8-hydroxylated $[8\text{-OH-G} + H]^{\bullet+}$, which was proposed on the basis of EPR/electron nuclear double resonance measurement of $OH^{\bullet}$ addition to a single crystal of N7-protonated guanine[32] and recently confirmed by the reaction of $G^{\bullet+}$ with water in the gas phase.[33,34] This structure mediates the formation of the most common base lesion 8-oxo-7,8-dihydroguanine.[35,36] Neutral $[G - H]^{\bullet}$, on the other hand, does not react with water[37] or lead to 8-oxo-7,8-dihydroguanine.[38] The products are dictated by the oxidation of $[G - H]^{\bullet}$ to a 5-hydroperoxide-guanine and then a 5-hydroxyl-guanine, followed by reduction to a spiroiminodihydantoin and a 5-carboxamido-5-formamido-2-iminohydantoin.[39] Alternatively, $[G - H]^{\bullet}$ may be oxidized to a 2,5-diaminoimidazolone and a 2,2,4-triamino-2*H*-oxazol-5-one.[40]

Very recently, we investigated the reaction of singlet oxygen ($^1O_2$) with radical cations of guanine, 9-methylguanine, 2′-deoxyguanosine and guanosine.[41] Singlet O_2 is one of the reactive oxygen species generated in living systems through enzymatic and nonenzymatic reactions, type II photosensitization, chemical excitation, and so forth.[42,43] Singlet O_2 causes DNA damage,[35,44−47] and lesions are initiated exclusively at the guanine residues.[35,44−68] Our work found that the $^1O_2$ oxidation of the guanine radical cation leads to the formation of an 8-peroxide,[41] from which a variety of products evolve. Note that under normal biological conditions, the encounter probability of $^1O_2$ with guanine radical species is low due to their low local concentrations and short lifetimes. However, the situation changes under strong cellular oxidative stress, which creates an imbalance between production and accumulation of reactive oxygen species in cells and the ability of a biological system to scavenge these reactive species. For example, ionizing radiation and/or one-electron oxidants interact with DNA in the presence of $^1O_2$. Such concurrent processes of $^1O_2$ and nucleobase radicals are in fact utilized in a combination of ionization radiation-based radiotherapy and $^1O_2$-based photodynamic therapy for cancer treatment, in which synergistic effects are anticipated.[69−71]

In the present work, we extend the study to the $^1O_2$ oxidation of $[9MG\cdot 1MC]^{\bullet+}$. The equilibrium ensemble of $9MG^{\bullet+}\cdot 1MC \rightleftharpoons [9MG - H]^{\bullet}\cdot[1MC + H]^{+}$ provides guanine in two different reactant structures. Guided by the prior understanding of $9MG^{\bullet+}$ with $^1O_2$, we sought to explore the following issues: (i) similarities and differences between the reactivities of $9MG^{\bullet+}$ versus $[9MG - H]^{\bullet}$ toward $^1O_2$, (ii) influence of Watson−Crick H-bonding on the $^1O_2$ oxidation product and energetic profile,

https://doi.org/10.1021/acs.jpcb.2c03748
J. Phys. Chem. B 2022, 126, 5458−5472

and (iii) influence of intra-base pair PT on $^1O_2$ oxidation and vice versa.

The paper is organized as follows. The experimental setup and methods are described in Section 2. Computational approaches are reported in Section 3. In Section 4, a previous experiment of $9MG^{\bullet+}$ with $^1O_2$ is recapitulated, followed by a new theoretical analysis of this system and comparison of singlet oxygenation of $9MG^{\bullet+}$ versus $[9MG - H]^{\bullet}$. We then present the experimental and theoretical results of $9MG^{\bullet+}\cdot 1MC \rightleftharpoons [9MG - H]^{\bullet}\cdot[1MC + H]^+$ with $^1O_2$. The biological implications of the present findings are discussed in Section 5, followed by conclusions in Section 6.

2. EXPERIMENTAL PROCEDURES

2.1. General. 9MG (Aldrich, 98%), 1MC (enamine, 95%), $Cu(NO_3)_2$ (Alfa Aesar, 99.999%), KOH (Fisher Chemical, > 85%), H_2O_2 (Acros Organics, 35 wt %), methanol (HPLC grade, Fisher Chemical), water (HPLC grade, J.T. Baker), Cl_2 (99.5%, Sigma-Aldrich), and He (99.995%, Praxair) were used as received.

Singlet O_2 was generated in the reaction of $H_2O_2 + Cl_2 + 2KOH \rightarrow {}^1O_2/{}^3O_2 + 2KCl + 2H_2O$.[72,73] Briefly, 10.5 mL of 8 M KOH was added to 20 mL of 35 wt % aqueous H_2O_2 in a sparger that was immersed in a chiller held at −18 °C. 3.42 sccm of Cl_2 was mixed with 53.5 sccm of He within a gas proportioner and bubbled through the H_2O_2/KOH slush. Cl_2 reacted completely with H_2O_2 and produced a mixture of $^1O_2$, $^3O_2$, and water. The gaseous products passed through a cold trap (kept at −70 °C) to remove water vapor. Only $^1O_2$, $^3O_2$, and He remained in the downstream gas. The absolute concentration of $^1O_2$ in the gas mixture was determined by measuring $^1O_2$ phosphorescence ($a^1\Delta_g \rightarrow X^3\Sigma g^-$) at 1270 nm using a photodetection system consisting of an emission cell, optical lenses, a 1270 nm interference filter, a thermoelectrically cooled InGaAs photodetector (Newport 71887), and a lock-in amplifier (Stanford Research Systems SR830).[74] A steady $^1O_2$ gas flow with a concentration of 15% was produced for conducting an ion-molecule reaction.

2.2. Formation of a Base Pair Radical Cation and Ion-Molecule Reactions. Recently, electrospray ionization (ESI)-tandem mass spectrometry has emerged as a new approach for the formation and reactions of nucleobase radical cations in the gas phase.[28,33,34,41,75−82] In this work, formation of $[9MG\cdot 1MC]^{\bullet+}$ and its reaction with $^1O_2$ were carried out on a home-made ESI guided-ion beam scattering tandem mass spectrometer. Details of the apparatus have been reported in our previous work.[33,83] A methanol/water (v/v = 3:1) solution of 9MG, 1MC, and $Cu(NO_3)_2$ in equimolar concentrations (0.25 mM) was freshly prepared and sprayed into the air through an ESI needle at a rate of 0.06 mL/h. The $[Cu^{II}(9MG)_n(1MC)_{4-n}]^{\bullet 2+}$ complexes[27] formed in the electrospray entered the source chamber of the mass spectrometer through a desolvation capillary which was heated up to 194 °C. A 1.0 mm-orifice skimmer was located 3 mm away from the end of the desolvation capillary, separating the source chamber and a hexapole ion guide. The capillary and skimmer were biased at 100 and 19 V, respectively, with respect to the ground. The electrical field between the capillary and the skimmer prompted redox charge separation-induced dissociation of $[Cu^{II}(9MG)_n(1MC)_{4-n}]^{\bullet 2+}$ upon collisions with background gas (1.7 τ) in the source chamber, from which $[9MG\cdot 1MC]^{\bullet+}$ was formed.[27,28,33,41,77,78] Monohydrated $[9MG\cdot 1MC]^{\bullet+}\cdot H_2O$ was produced in a similar manner except that the ESI solution was made in a 2:1 methanol/water mixture.

Radical cations were transported into the hexapole ion guide for collisional focusing, energy dumping, and thermalization to 310 K, followed by mass selection in a quadrupole mass filter. After the mass section, ion beam intensities were 5×10^4 counts/s for $[9MG\cdot 1MC]^{\bullet+}$ and 1×10^4 counts/s for $[9MG\cdot 1MC]^{\bullet+}\cdot H_2O$. The initial kinetic energy of the ion beam was 0.9 eV in the laboratory frame with a full width at half-maximum of 0.6 eV, as measured using retarding potential analysis[84] at the entrance of an octopole ion guide. The mass-selected ion beam was then injected into the octopole that passed through a scattering cell containing reactant gas. In addition to providing radio frequency potential that trapped ions in the radial direction, the octopole ion guide was biased at a variable DC potential. The DC offset decelerated or accelerated the mass-selected ion beam to a well-defined kinetic energy in the laboratory frame (E_{lab}), thereby controlling the collision energy (E_{col}) between radical cations and $^1O_2$ in the center-of-mass frame, as $E_{col} = E_{lab} \times m_{neutral}/(m_{ion} + m_{neutral})$ where m_{ion} and $m_{neutral}$ denote the masses of ionic and neutral reactants, respectively. The scattering cell pressure was maintained at 0.25 mτ (including $^1O_2$, $^3O_2$, and He). At this pressure, guanine radical cations had at most single collisions with O_2.

Product ions resulting from the ion-molecule reaction and the remaining reactant ions were collected by the octopole, passed into a second quadrupole mass filter for mass analysis, and extracted toward a pulse-counting electron multiplier detector. As ion-molecule collisions were carried out in a thin-target limit that is analogous to the Beer−Lambert law,[85] the reaction cross section could be calculated from the ratio of product/reactant ion intensities at each E_{col}, the pressure and the concentration of $^1O_2$ in the scattering cell, and the effective cell length. Note that the guanine radical cation does not react with $^3O_2$,[86] as we verified in a control experiment using pure $^3O_2$ as the reactant gas.

3. COMPUTATIONAL ANALYSIS

3.1. Approximately Spin-Projected DFT. Geometries of reaction structures including reactants, intermediates, transition states (TSs), and products were fully optimized at the unrestricted ωB97XD/6-31+G(d,p) level of theory. This range-separated functional was chosen as it mitigates self-interaction errors and improves the orbital description of radical ions[87] than the B3LYP functional, the latter introducing severe spin contamination in the guanine radical cation.[37] Vibrational frequencies were calculated to confirm that stationary points are energy minima on the reaction potential energy surface (PES) with no imaginary frequency, while TSs are first-order saddle points and their only imaginary frequencies represent the anticipated reaction coordinates. Intrinsic reaction coordinate calculations were carried out to further ascertain that TSs are connected to correct reactant/product minima. Basis set superposition errors (BSSEs, which occur when a finite basis set stabilizes the base pair more than the separate bases and thus overestimates the base pairing energy)[88] were calculated to be <0.05 eV using the counterpoise method[89,90] and have been corrected for in reaction PES. DFT calculations (including spin densities and ESP maps) were accomplished using Gaussian 16.[91]

The calculation of the reaction PES for a radical with $^1O_2$ is challenged by multi-configuration wavefunctions originating from the mixed open- and closed-shell character of $^1O_2$.[92] The spin-restricted DFT cannot describe the static correlation arising from the two degenerate π^* orbitals and overestimates

https://doi.org/10.1021/acs.jpcb.2c03748
J. Phys. Chem. B 2022, 126, 5458−5472

the $^1O_2$ excitation energy by 0.7 eV, whereas the unrestricted broken spin-symmetry DFT brings about spin contamination from $^3O_2$ and underestimates the excitation by 0.5 eV.[93−95] This problem affects not only the $^1O_2$ reactant but also the intermediates and TSs for $^1O_2$ addition to the guanine radical.[41,79,80] In the latter case, the target doublet state ^{2}[[9MG·1MC]$^{\bullet+}(\uparrow)\cdots{}^1O_2(\uparrow\downarrow)$] not only suffers from spin contamination of a lower-energy lying quartet state ^{4}[[9MG·1MC]$^{\bullet+}(\uparrow)\cdots{}^3O_2(\uparrow\uparrow)$] but also mistakenly converges to a lower-energy but incorrect doublet state ^{2}[[9MG·1MC]$^{\bullet+}(\downarrow)\cdots{}^3O_2(\uparrow\uparrow)$].

To avoid crossing to ^{2}[[9MG·1MC]$^{\bullet+}(\downarrow)\cdots{}^3O_2(\uparrow\uparrow)$], charges and spins of individual fragments in ^{2}[[9MG·1MC]$^{\bullet+}(\uparrow)\cdots{}^1O_2(\uparrow\downarrow)$] were specified using guess = fragments in the DFT calculation. To correct for spin contaminations in $^1O_2$ and $^1O_2$-adducts, Yamaguchi's approximate spin projection scheme[96] was applied. The spin-projected DFT energy is given by

$$E = \frac{\langle \hat{\mathbf{S}}^2\rangle^{\mathrm{HS}} - \langle \hat{\mathbf{S}}^2\rangle^{\mathrm{BS}}_{\mathrm{exact}}}{\langle \hat{\mathbf{S}}^2\rangle^{\mathrm{HS}} - \langle \hat{\mathbf{S}}^2\rangle^{\mathrm{BS}}} E^{\mathrm{BS}} - \frac{\langle \hat{\mathbf{S}}^2\rangle^{\mathrm{BS}} - \langle \hat{\mathbf{S}}^2\rangle^{\mathrm{BS}}_{\mathrm{exact}}}{\langle \hat{\mathbf{S}}^2\rangle^{\mathrm{HS}} - \langle \hat{\mathbf{S}}^2\rangle^{\mathrm{BS}}} E^{\mathrm{HS}} \quad (1)$$

where E^{BS} and $\langle \hat{\mathbf{S}}^2\rangle^{\mathrm{BS}}$ refer to the energy and the average value of the total spin angular momentum operator for the broken-symmetry, low-spin target state (before annihilation of spin contamination) and E^{HS} and $\langle \hat{\mathbf{S}}^2\rangle^{\mathrm{HS}}$ represent counterparts for the high-spin state. When spin contamination is negligible, $\langle \hat{\mathbf{S}}^2\rangle^{\mathrm{BS}}$ is close to its exact value $\langle \hat{\mathbf{S}}^2\rangle^{\mathrm{BS}}_{\mathrm{exact}}$ defined as

$$\langle \hat{\mathbf{S}}^2\rangle^{\mathrm{BS}}_{\mathrm{exact}} = \frac{N^\alpha - N^\beta}{2}\left(\frac{N^\alpha - N^\beta}{2} + 1\right) \quad (2)$$

where N^α and N^β are the numbers of α and β electrons, respectively. $\langle \hat{\mathbf{S}}^2\rangle^{\mathrm{BS}}_{\mathrm{exact}}$ is zero for $^1O_2$ and 0.75 for radical−$^1O_2$ adducts.[80]

3.2. Coupled-Cluster Theory. Besides the $\langle \hat{\mathbf{S}}^2\rangle$ assessment at ωB97XD/6-31+G(d,p), the domain-based local pair-natural orbital coupled-cluster single-, double-, and perturbative triple-excitations method DLPNO-CCSD(T)[97] coupled with the aug-cc-pVQZ basis set[98,99] was employed to assess the spin contamination in the reaction structures using the T1 diagnostic,[100,101] wherein $T_1 = \|t_1\|/\sqrt{n}$ (i.e., the Frobenius norm of the single-excitation amplitude vector divided by the square root of the number of electrons correlated). Empirically, a T1 value that is greater than 0.02 for a closed-shell system or greater than 0.03 for an open-shell system indicates severe multiconfigurational characters or nondynamical correlation effects, which require other important configurations as references in the treatment of nondynamic electron correlation.[100]

The inclusion of a perturbative correction for triple excitation in CCSD(T) compensates for the deficiencies of a single-determinant reference to some extent. Therefore, DLPNO-CCSD(T) is able to partially include non-dynamical correlation effects. For closed-shell systems, the coupled-cluster theory is considered as a gold standard[102] of quantum chemistry with its accuracy comparable to experiments. The DLPNO-CCSD(T) T1 diagnostic and energy calculations were carried out using ORCA ver. 4.2.[103]

3.3. Multi-Reference Active Space Self-Consistent Field Method. To cross check the reliability of different theories in the treatment of radical−$^1O_2$ interactions, reactions of $^1O_2$ with monomeric 9MG$^{\bullet+}$ and [9MG − H]$^\bullet$ were subjected to the multi-reference active space self-consistent field method CASPT2/6-31G(d,p) calculations.[104,105] Compared to the complete active space self-consistent field (CASSCF)[106] method that treats electron correlation energy in an unbalanced way by considering only those that correspond to active orbitals (i.e., static correlation), CASPT2 adds dynamical correlation to the CASSCF wave function using the second-order perturbation theory. The additional dynamical correlation is essential for modeling the $^1O_2$ reaction with guanine, as the CASSCF method significantly overestimated the reaction activation barriers and product energies for neutral guanine,[63] 9MG$^{\bullet+}$[41] and 9-methyl-8-oxoguanine radical cation (9MOG$^{\bullet+}$).[79] On the other hand, the CASPT2 method provided reliable reaction energetics for $^1O_2$ with 9MG$^{\bullet+}$, 9MOG$^{\bullet+}$, and 8-bromoguanine radical cation (8BrG$^{\bullet+}$).[80]

CASPT2 calculations were carried out using OpenMolcas ver. 21.06.[107,108] The shift parameter for ionization potential-electron affinity was set to 0.25 a.u.[109] The size of the active space was (9, 7) for 9MG$^{\bullet+}$ and [9MG − H]$^\bullet$, (12, 8) for $^1O_2$, and (21, 15) for the adducts. The active space included the O_2 $\sigma_{O(2s)-O(2s)}$, $\sigma^*_{O(2s)-O(2s)}$, $\sigma_{O(2p)-O(2p)}$, $\pi_{\pm1}$, $\pi^*_{\pm1}$, and $\sigma^*_{O(2p)-O(2p)}$ orbitals and the guanine π orbitals that participate in and/or affect the $^1O_2$-addition. The reaction enthalpy (ΔH) reported in this work is based on the sum of electronic energy calculated at a specific level and thermal correction to 298 K calculated at ωB97XD/6-31+G(d,p), including the zero-point energy, which was scaled by a factor of 0.975.[110]

4. RESULTS AND DISCUSSION

4.1. Singlet Oxygenation of Monomeric 9MG$^{\bullet+}$ versus [9MG − H]$^\bullet$. *4.1.1. Review of the 9MG$^{\bullet+}$ Reaction with $^1O_2$.* Before examining the singlet oxygenation of a base pair, the findings from monomeric 9MG$^{\bullet+}$ with $^1O_2$ are recapitulated.[41] A 9MG$^{\bullet+}$-O_2 adduct was detected in the $^1O_2$ oxidation of 9MG$^{\bullet+}$. The reaction is exothermic and barrierless. In fact, the large reaction heat release had decomposed most of the 9MG$^{\bullet+}$-O_2 adduct within a time scale shorter than the mass spectrometer time-of-flight ($\sim10^2$ μs). As a consequence, the majority of product ions escaped mass spectrometric detection. In order to overcome this unfavorable reaction kinetics, monohydrated 9MG$^{\bullet+}$·H_2O was used instead. In this case, heat release from the $^1O_2$ addition was used up mostly for eliminating the water ligand and for product kinetic energy release, which in turn relaxed the internal excitation energy and, thus, stabilized the 9MG$^{\bullet+}$-O_2 product. Reaction efficiency, estimated by the ratio of the reaction cross section to the Langevin ion-capture cross section,[111] was maximum (1.4%) at the lowest experimental E_{col} (0.05 eV), decreased with increasing E_{col} and became negligible above 0.6 eV. This indicates that the reaction is mediated by a complex which becomes short-lived and insignificant at high energies.

4.1.2. New Theoretical Results. In our previous work,[41] a conventional ωB97XD/6-31+G(d,p) method was utilized to identify reaction pathways for 9MG$^{\bullet+}$ + $^1O_2$, augmented by single-point energy calculations at DLPNO-CCSD(T)/aug-cc-pVTZ, CASSCF(21,15)/6-31+G(d,p), and CASPT2(21,15)/6-31G(d,p). In the present work, we have reoptimized reaction structures using spin-unrestricted ωB97XD/6-31+G(d,p), recalculated DFT energies using approximate spin projection, and refined DLPNO-CCSD(T) energies using a large basis set

https://doi.org/10.1021/acs.jpcb.2c03748
J. Phys. Chem. B 2022, 126, 5458−5472

Scheme 2. Probable Pathways and Products for the $^1O_2$ Oxidation of $9MG^{\bullet+}$ and $9MG^{\bullet+}\cdot1MC$, in which Dashed Lines Represent Intra-Base Pair H-Bonding

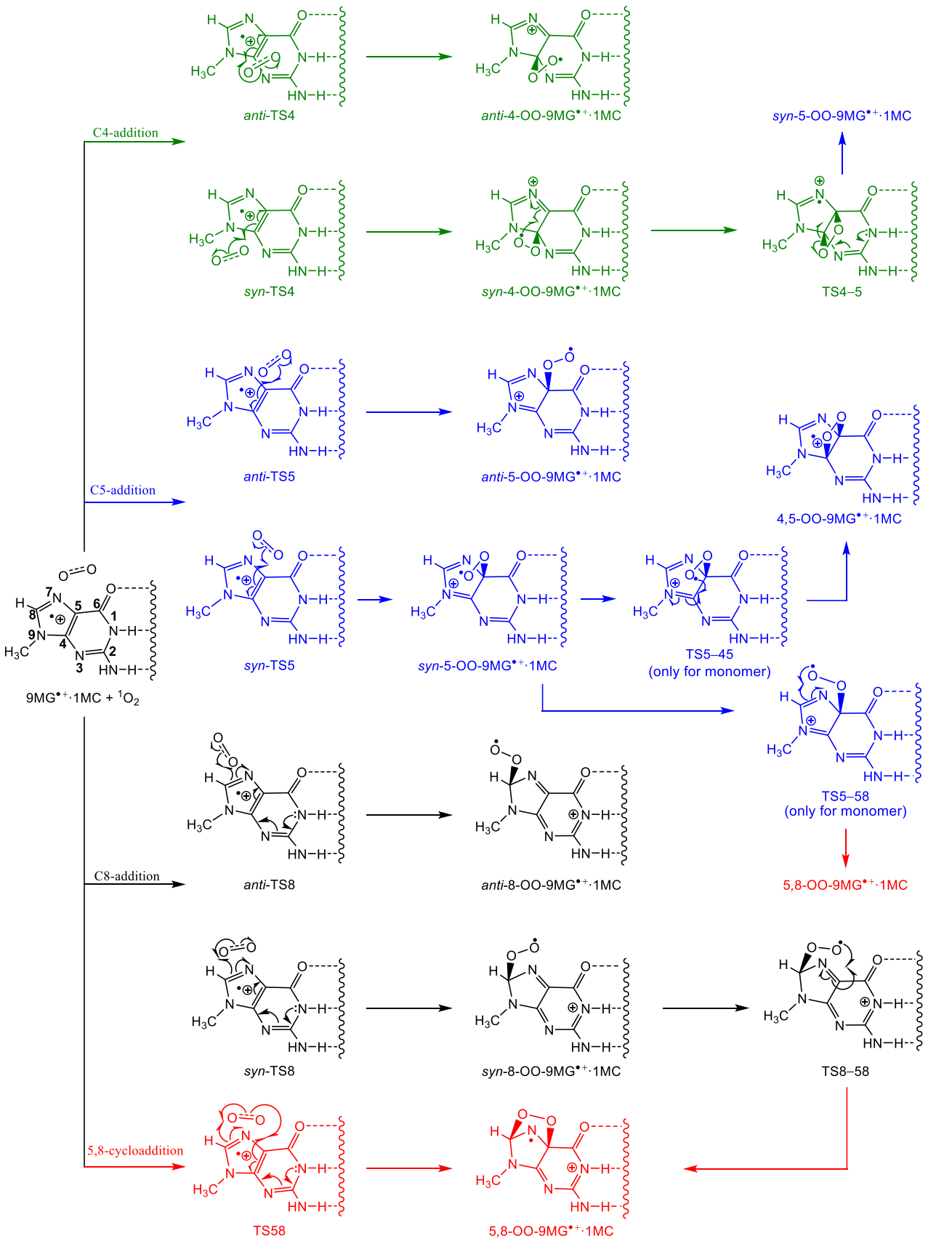

https://doi.org/10.1021/acs.jpcb.2c03748
J. Phys. Chem. B 2022, 126, 5458−5472

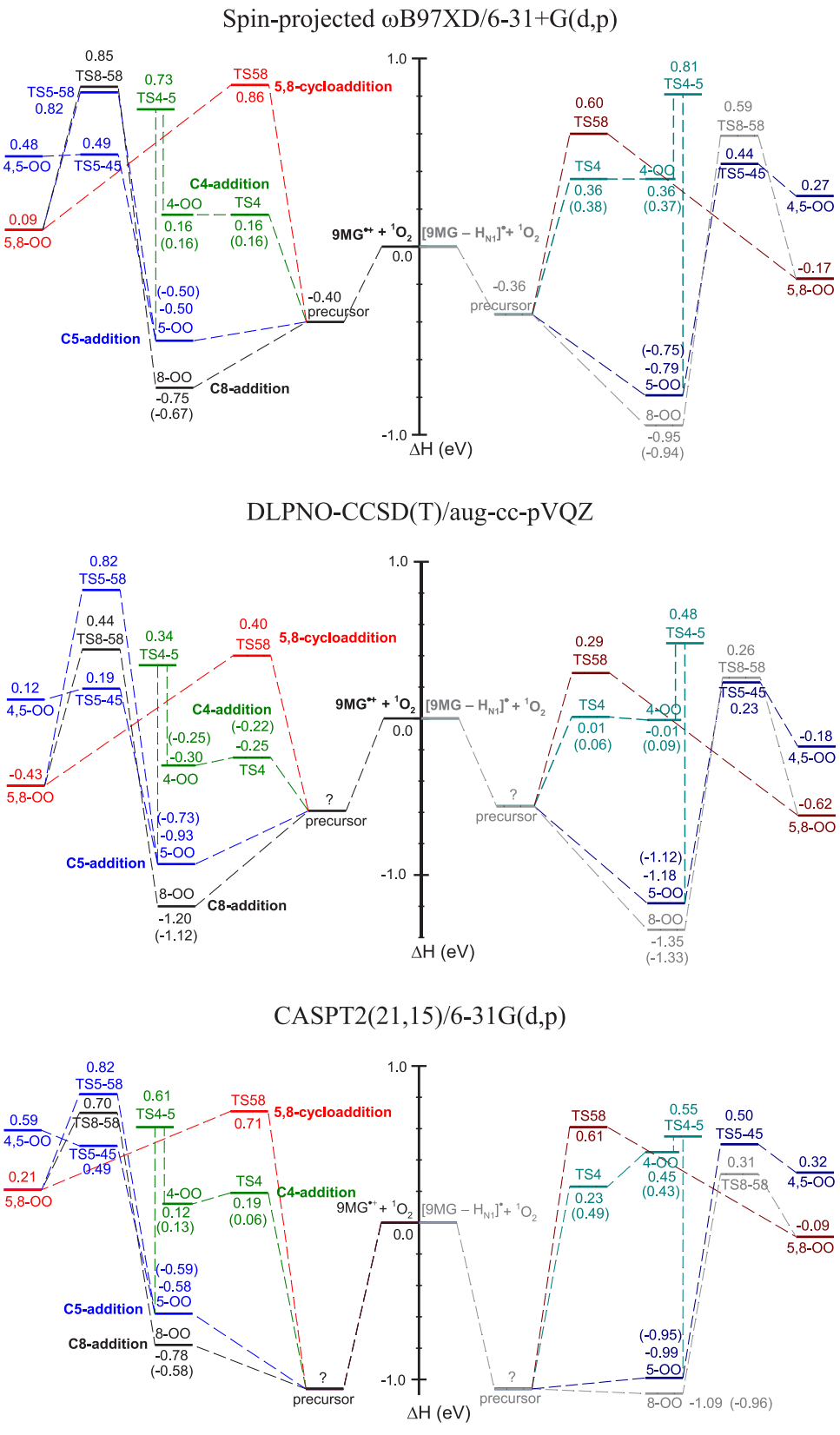

Figure 1. Reaction PES for (left) $9MG^{\bullet+}$ + $^1O_2$ and (right) $[9MG - H]^{\bullet}$ + $^1O_2$ calculated at different levels of theory (DLPNO-CCSD(T) and CASPT2 failed to locate a correct precursor, as discussed in the main text). For 4-, 5-, and 8-peroxides and corresponding TSs, enthalpies for both *syn*- and *anti*-conformers are provided, with the *anti* listed in parentheses.

aug-cc-pVQZ. Reaction structures are depicted in Scheme 2. Note that in view of the similarities between the reactions of $9MG^{\bullet+}$ and $9MG^{\bullet+}$·1MC (vide infra), the scheme combines the two reaction systems wherein dashed lines represent H-bonding

https://doi.org/10.1021/acs.jpcb.2c03748
J. Phys. Chem. B 2022, 126, 5458−5472

Table 1. Energies (eV) of Reaction Species Calculated at Different Levels of Theory[a]

radical cations	ωB97XD /6-31+G**	DLPNO-CCSD(T) /aug-cc-pVQZ	CASPT2(21,15) /6-31G**	neutral radical	ωB97XD /6-31+G**	DLPNO-CCSD(T) /aug-cc-pVQZ	CASPT2(21,15) /6-31G**
$9MG^{\bullet+} + {}^1O_2$	0.00	0.00	0.00	$[9MG-H]^{\bullet} + {}^1O_2$	0.00	0.00	0.00
	0.00	0.00	–		0.00	0.00	–
precursor	-0.40	–	–	precursor	-0.36	–	–
	-0.38	–	–		-0.37	–	–
C4-addition							
syn-TS4	0.16	-0.25	0.19	*syn*-TS4	0.36	0.01	0.23
	0.34	-0.05	–		0.35	-0.03	–
syn-[4-OO-9MG]$^{\bullet+}$	0.16	-0.30	0.12	*syn*-[4-OO-9MG – H]$^{\bullet}$	0.37	-0.01	0.45
	0.34	-0.09	–		0.35	-0.07	–
rot-TS4	0.27	-0.20	0.20	rot-TS4	0.51	0.14	0.43
	0.43	0.01	–		0.45	0.04	–
anti-TS4	0.16	-0.22	0.06	*anti*-TS4	0.38	0.06	0.49
	0.32	-0.04	–		0.34	-0.01	–
anti-[4-OO-9MG]$^{\bullet+}$	0.16	-0.25	0.13	*anti*-[4-OO-9MG – H]$^{\bullet}$	0.37	0.09	0.43
	0.35	-0.03	–		0.37	0.01	–
TS4–5	0.73	0.34	0.61	TS4–5	0.81	0.48	0.55
	0.83	0.47	–		0.84	0.47	–
C5-addition							
syn-TS5	-0.50	-0.84	-0.62	*syn*-TS5	-0.57	-0.96	-0.98
	-0.52	-0.85	–		-0.56	-0.89	–
syn-[5-OO-9MG]$^{\bullet+}$	-0.50	-0.93	-0.58	*syn*-[5-OO-9MG – H]$^{\bullet}$	-0.79	-1.18	-0.99
	-0.54	-0.95	–		-0.61	-1.01	–
rot-TS5	-0.43	-0.86	-0.53	rot-TS5	-0.73	-1.11	-0.92
	-0.48	-0.88	–		-0.54	-0.94	–
anti-TS5	-0.43	-0.78	-0.71	*anti*-TS5	-0.59	-0.89	-0.93
	-0.46	-0.80	–		-0.51	-0.85	–
anti-[5-OO-9MG]$^{\bullet+}$	-0.50	-0.92	-0.59	*anti*-[5-OO-9MG – H]$^{\bullet}$	-0.75	-1.12	-0.95
	-0.54	-0.94	–		-0.60	-1.00	–
C8-addition							
syn-TS8	-0.58	-0.99	-0.84	*syn*-TS8	-0.72	-1.01	-0.95
	-0.69	-0.95	–		-0.71	-0.96	–
syn-[8-OO-9MG]$^{\bullet+}$	-0.75	-1.20	-0.78	*syn*-[8-OO-9MG – H]$^{\bullet}$	-0.95	-1.35	-1.09
	-0.76	-1.19	–		-0.80	-1.23	–
rot-TS8	-0.52	-0.96	-0.54	rot-TS8	-0.74	-1.12	-0.87
	-0.53	-0.94	–		-0.57	-0.98	–
anti-TS8	-0.39	-0.63	-0.50	*anti*-TS8	-0.51	-0.69	-0.61
	-0.37	-0.59	–		-0.39	-0.61	–
anti-[8-OO-9MG]$^{\bullet+}$	-0.67	-1.12	-0.58	*anti*-[8-OO-9MG – H]$^{\bullet}$	-0.94	-1.33	-0.96
	-0.69	-1.13	–		-0.74	-1.20	–
5,8-cycloaddition							
TS58	0.86	0.40	0.71	TS58	0.60	0.29	0.61
	0.82	0.40	–		0.76	0.39	–
[5,8-OO-9MG]$^{\bullet+}$	0.09	-0.43	0.21	[5,8-OO-9MG – H]$^{\bullet}$	-0.17	-0.62	-0.09
	0.06	-0.43	–		-0.005	-0.49	–
TS5–58	0.82	0.82	0.82	TS5–58	N/A	N/A	–
	N/A	N/A	–		N/A	N/A	–
TS8–58	0.85	0.44	0.70	TS8–58	0.59	0.26	0.31
	0.76	0.44	–		0.76	0.31	–
4,5-dioxetane							
TS5–45	0.49	0.19	0.49	TS5–45	0.44	0.23	0.50
	N/A	N/A	–		0.61	0.52	–
[4,5-OO-9MG]$^{\bullet+}$	0.48	0.12	0.59	[4,5-OO-9MG – H]$^{\bullet}$	0.27	-0.18	0.32
	N/A	N/A	–		0.59	0.27	–

[a]Values for base pairs are shown in the gray shaded area.

in $9MG^{\bullet+}$·1MC and should be ignored for a monomeric $9MG^{\bullet+}$. Their Cartesian coordinates are provided in the Supporting Information.

The reaction is initiated at a precursor complex $^2[9MG^{\bullet+}(\uparrow)\cdots{}^1O_2(\uparrow\downarrow)]$, from which four pathways may evolve. The first three pathways represent C4-, C5-, and C8-terminal additions, each of which is illustrated in green, blue, and black colors, respectively, in Scheme 2. Each addition leads to a peroxide structure with *syn*- and *anti*-configurations with respect to the imidazole ring. For example, the C8-addition produces a *syn*-[8-OO-9MG]$^{\bullet+}$ via an activation barrier *syn*-TS8 and *anti*-[8-OO-9MG]$^{\bullet+}$ via *anti*-TS8. The pair of rotamers may interconvert via a rotation barrier rot-TS8 (not shown in the scheme). The structures of [8-OO-9MG]$^{\bullet+}$ have a radical site on

https://doi.org/10.1021/acs.jpcb.2c03748
J. Phys. Chem. B 2022, 126, 5458−5472

Table 2. $\langle \hat{S}^2 \rangle$ and T1 Diagnostic for Reaction Species along with Their Energy Differences between Different Levels of Theory[a]

radical cations	$\langle \hat{S}^2 \rangle$	T1	$\Delta_{CCSD(T)\text{-}\omega B97XD}$	$\Delta_{CASPT2\text{-}\omega B97XD}$	neutral radicals	$\langle \hat{S}^2 \rangle$	T1	$\Delta_{CCSD(T)\text{-}\omega B97XD}$	$\Delta_{CASPT2\text{-}\omega B97XD}$
$9MG^{\bullet+} + {}^1O_2$	0.767 [a]	0.019 [a]	0.00	0.00	$[9MG - H]^{\bullet} + {}^1O_2$	0.776 [a]	0.018 [a]	0.00	0.00
	0.768 [a]	0.017 [a]	0.00	0.00		0.768 [a]	0.016 [a]	0.00	0.00
precursor	1.717	–	–	–	precursor	1.750	–	–	–
	1.731	–	–	–		1.733	–	–	–
C4-addition									
syn-TS4	0.760	0.020	-0.41	0.03	*syn*-TS4	0.760	0.021	-0.35	-0.13
	0.759	0.018	-0.39	–		0.759	0.018	-0.38	–
syn-$[4\text{-OO-9MG}]^{\bullet+}$	0.754	0.019	-0.46	-0.04	*syn*-$[4\text{-OO-9MG} - H]^{\bullet}$	0.755	0.021	-0.38	0.08
	0.754	0.018	-0.43	–		0.755	0.018	-0.42	–
rot-TS4	0.754	0.019	-0.47	-0.07	rot-TS4	0.755	0.020	-0.37	-0.08
	0.754	0.018	-0.42	–		0.755	0.018	-0.41	–
anti-TS4	0.763	0.020	-0.38	-0.1	*anti*-TS4	0.757	0.021	-0.32	0.11
	0.758	0.018	-0.36	–		0.757	0.018	-0.35	–
anti-$[4\text{-OO-9MG}]^{\bullet+}$	0.755	0.019	-0.41	-0.03	*anti*-$[4\text{-OO-9MG} - H]^{\bullet}$	0.755	0.021	-0.28	0.06
	0.756	0.018	-0.38	–		0.756	0.018	-0.36	–
TS4–5	0.757	0.021	-0.39	-0.12	TS4–5	0.758	0.021	-0.33	-0.26
	0.757	0.019	-0.36	–		0.757	0.019	-0.37	–
C5-addition									
syn-TS5	0.807	0.019	-0.34	-0.12	*syn*-TS5	0.892	0.019	-0.39	-0.41
	0.825	0.018	-0.33	–		0.846	0.018	-0.33	–
syn-$[5\text{-OO-9MG}]^{\bullet+}$	0.754	0.019	-0.43	-0.08	*syn*-$[5\text{-OO-9MG} - H]^{\bullet}$	0.754	0.020	-0.39	-0.20
	0.754	0.018	-0.41	–		0.754	0.018	-0.40	–
rot-TS5	0.755	0.019	-0.43	-0.10	rot-TS5	0.755	0.020	-0.38	-0.19
	0.755	0.018	-0.40	–		0.755	0.018	-0.40	–
anti-TS5	0.892	0.019	-0.35	-0.28	*anti*-TS5	0.955	0.019	-0.30	-0.34
	0.898	0.018	-0.34	–		0.914	0.018	-0.34	–
anti-$[5\text{-OO-9MG}]^{\bullet+}$	0.755	0.019	-0.42	-0.09	*anti*-$[5\text{-OO-9MG} - H]^{\bullet}$	0.755	0.020	-0.37	-0.20
	0.755	0.018	-0.40	–		0.755	0.018	-0.40	–
C8-addition									
syn-TS8	0.807	0.020	-0.41	-0.26	*syn*-TS8	0.967	0.020	-0.29	-0.23
	0.901	0.018	-0.26	–		0.920	0.018	-0.25	–
syn-$[8\text{-OO-9MG}]^{\bullet+}$	0.754	0.019	-0.45	-0.03	*syn*-$[8\text{-OO-9MG} - H]^{\bullet}$	0.754	0.019	-0.40	-0.14
	0.754	0.017	-0.43	–		0.754	0.017	-0.43	–
rot-TS8	0.754	0.018	-0.44	-0.02	rot-TS8	0.754	0.019	-0.38	-0.13
	0.754	0.017	-0.41	–		0.754	0.017	-0.41	–
anti-TS8	1.047	0.019	-0.24	-0.11	*anti*-TS8	1.136	0.019	-0.18	-0.10
	1.068	0.017	-0.22	–		1.090	0.017	-0.22	–
anti-$[8\text{-OO-9MG}]^{\bullet+}$	0.754	0.018	-0.45	0.09	*anti*-$[8\text{-OO-9MG} - H]^{\bullet}$	0.754	0.019	-0.39	-0.02
	0.754	0.017	-0.44	–		0.754	0.018	–0.46	–
5,8-cycloaddition									
TS58	0.777	0.018	-0.46	-0.15	TS58	0.772	0.025	-0.31	0.01
	0.773	0.017	-0.42	–		0.772	0.021	-0.37	–
$[5,8\text{-OO-9MG}]^{\bullet+}$	0.756	0.016	-0.52	0.12	$[5,8\text{-OO-9MG} - H]^{\bullet}$	0.756	0.016	-0.45	0.08
	0.756	0.015	-0.49	–		0.756	0.016	-0.49	–
TS5–58	0.759	0.046	0.00	0.00	TS5–58	N/A	N/A	–	–
	N/A	N/A	–	–		N/A	N/A	–	–
TS8–58	0.827	0.022	-0.41	-0.15	TS8–58	0.817	0.022	-0.33	-0.28
	0.824	0.020	-0.32	–		0.821	0.020	-0.45	–
4,5-dioxetane									
TS5–45	0.760	0.025	-0.30	0.00	TS5–45	0.768	0.026	-0.21	0.06
	N/A	N/A	–	–		0.764	0.025	-0.09	–
$[4,5\text{-OO-9MG}]^{\bullet+}$	0.773	0.022	-0.36	0.11	$[4,5\text{-OO-9MG} - H]^{\bullet}$	0.775	0.018	-0.45	0.05
	N/A	N/A	–	–		0.762	0.017	-0.32	–

[a]Values for base pairs are shown in the gray shaded area. [b]The values refer to the guanine reactant; for ${}^1O_2$, $\langle \hat{S}^2 \rangle = 0$ and $T_1 = 0.015$.

the O_2 moiety. These peroxide radicals are quite reactive and able to abstract a hydrogen atom in DNA, particularly considering that the C8 of guanine has access to the sugar moiety as a likely abstraction site.[112] Note that $[4\text{-OO-9MG}]^{\bullet+}$ and $[5\text{-OO-9MG}]^{\bullet+}$ may interconvert via TS4–5, and $[5\text{-OO-9MG}]^{\bullet+}$ may transform to a 4,5-dioxetane via TS5–45. The fourth pathway is a concerted cycloaddition of O_2 across the imidazole C5–C8 bond via TS58, leading to the formation of a $[5,8\text{-OO-9MG}]^{\bullet+}$ endoperoxide, as illustrated in red color in the scheme. $[5,8\text{-OO-9MG}]^{\bullet+}$ may also form from $[8\text{-OO-9MG}]^{\bullet+}$ via TS8–58. No feasible pathway was found for 4,8-cycloaddition despite this being the most likely pathway in the ${}^1O_2$ reaction with neutral guanine/guanosine.[48,63]

https://doi.org/10.1021/acs.jpcb.2c03748
J. Phys. Chem. B 2022, 126, 5458–5472

Scheme 3. Doublet and Quartet $9MG^{\bullet+}\cdots O_2$ and $[9MG - H]^{\bullet}\cdots O_2$ Complexes with Spin Density Distributions Calculated at ωB97XD/6-31+G(d,p)

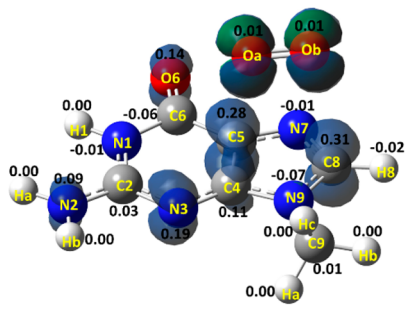

$^2[9MG^{\bullet+}(\uparrow, S = \frac{1}{2})\cdots{}^1O_2(\uparrow\downarrow, S = 0)]$

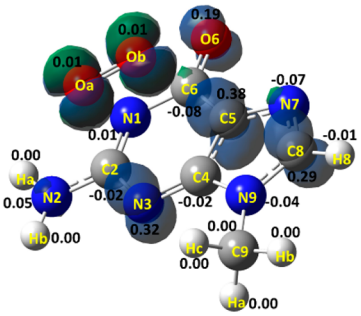

$^2[[9MG - H]^{\bullet}(\uparrow, S = \frac{1}{2})\cdots{}^1O_2(\uparrow\downarrow, S = 0)]$

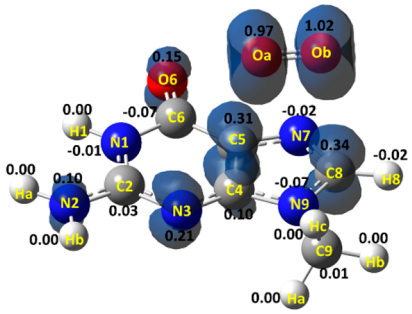

$^4[9MG^{\bullet+}(\uparrow, S = \frac{1}{2})\cdots{}^3O_2(\uparrow\uparrow, S = 1)]$

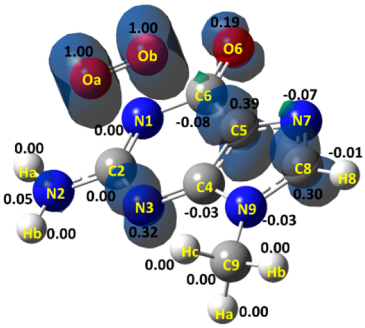

$^4[[9MG - H]^{\bullet}(\uparrow, S = \frac{1}{2})\cdots{}^3O_2(\uparrow\uparrow, S = 1)]$

Figure 1 shows a comparison of the reaction PES profiles constructed at three different levels of theory: spin-projected ωB97XD/6-31+G(d,p), DLPNO-CCSD(T)/aug-cc-pVQZ, and CASPT2(21,15)/6-31G(d,p). Table 1 reports reaction energetics for each pathway calculated at these levels. Table 2 reports $\langle\hat{S}^2\rangle$ and T1 values, $\Delta_{\text{DLPNO-CCSD(T)}-\omega\text{B97XD}}$ (i.e., the difference between the DLPNO-CCSD(T)- and spin-projected ωB97XD-calculated enthalpies), and $\Delta_{\text{CASPT2}-\omega\text{B97XD}}$ for each species. The $\langle\hat{S}^2\rangle$ and T1 diagnostic allow us to view how a multi-reference character evolves along individual pathways.

Besides the $^1O_2$ reactant, the precursor complex ($\langle\hat{S}^2\rangle$ = 1.717) presents severe multiconfigurational effects. A cautionary note in modeling a $^1O_2$ reaction with a doublet state is that according to spin density analysis, the lowest-energy doublet precursor complex in the DLPNO-CCSD(T) and CASPT2 calculations corresponds to a $^2[9MG^{\bullet+}(\downarrow)\cdots{}^3O_2(\uparrow\uparrow)]$ rather than a $^2[9MG^{\bullet+}(\uparrow)\cdots{}^1O_2(\uparrow\downarrow)]$. For this reason, the energies of precursor complexes at these two levels are indicated by question marks in Figure 1.

The correct doublet state $^2[9MG^{\bullet+}(\uparrow)\cdots{}^1O_2(\uparrow\downarrow)]$ was obtained by using a direct sum of $9MG^{\bullet+}(\uparrow)$ and $^1O_2(\uparrow\downarrow)$ as an initial guess, as visualized in Scheme 3. The $\langle\hat{S}^2\rangle$ value of $^2[9MG^{\bullet+}(\uparrow)\cdots{}^1O_2(\uparrow\downarrow)]$ indicates that this configuration is a mixture of a pure doublet ($\langle\hat{S}^2\rangle$ = 0.75) and a pure quartet ($\langle\hat{S}^2\rangle$ = 3.75). For this reason, a $^4[9MG^{\bullet+}(\uparrow)\cdots{}^3O_2(\uparrow\uparrow)]$ state was included in the approximate spin projection of the precursor (see Scheme 3).

Large $\langle\hat{S}^2\rangle$ and, concurrently, large $\Delta_{\text{CASPT2}-\omega\text{B97XD}}$ (−0.26 − −0.28 eV) were also observed in *syn*-TS8 and *anti*-TS5 (see Table 2). Relievingly, at all levels of theory, energies of TS5 and TS8 fall below that of the precursor complex. This indicates that C5- and C8-additions are actually barrierless, rendering TS5 and TS8 irrelevant (and thus not shown in Figure 1). The remaining intermediates and TSs have $\Delta_{\text{CASPT2}-\omega\text{B97XD}}$ within 0.15 eV, indicating good agreement between the two theories.

On the other hand, reaction structures present large $\Delta_{\text{DLPNO-CCSD(T)}-\omega\text{B97XD}}$, which ranges from −0.24 to −0.52 eV. DLPNO-CCSD(T) also predicted significantly higher reaction barriers and product energies in the $^1O_2$ reaction with $9MOG^{\bullet+}$ than ωB97XD and CASPT2.[79] It indicates that DLPNO-CCSD(T) is insufficient to describe the electronic structure of a completely degenerated system due to the lack of an adequate non-dynamical correlation.

In sum, all three theories have reached a qualitative agreement in terms of reaction pathways and all have identified $[8\text{-OO-}9MG]^{\bullet+}$ as the most probable product ion. The spin-projected ωB97XD and CASPT2 are able to produce quantitatively consistent PES. The formation exothermicity (−0.75 − −0.78 eV) of *syn*-$[8\text{-OO-}9MG]^{\bullet+}$ is higher than the $9MG^{\bullet+}\cdot H_2O$ binding energy (0.7 eV),[41] which rationalizes the experimental finding of $9MG^{\bullet+}\cdot H_2O + {}^1O_2 \rightarrow [8\text{-OO-}9MG]^{\bullet+} + H_2O$.

4.1.3. [9MG − H]$^{\bullet}$ versus 9MG$^{\bullet+}$. Figure 1 shows the PES for $[9MG - H]^{\bullet} + {}^1O_2$ constructed at the same levels of theory as

https://doi.org/10.1021/acs.jpcb.2c03748
J. Phys. Chem. B 2022, 126, 5458−5472

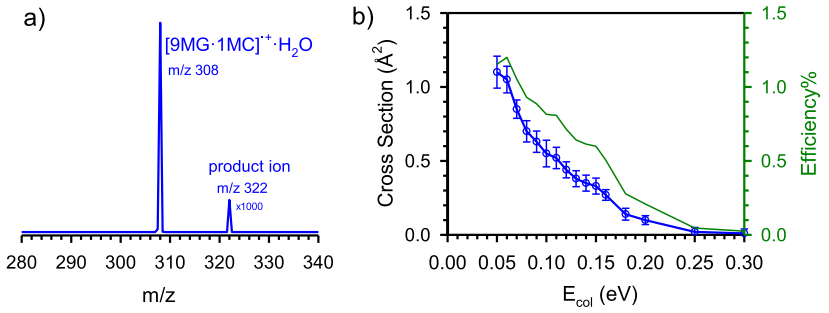

Figure 2. (a) Product ion mass spectrum for $[9MG{\cdot}1MC]^{\bullet+}{\cdot}H_2O + {}^1O_2$ acquired at E_{col} = 0.05 eV and (b) product ion cross section and reaction efficiency (right axis) as a function of E_{col}.

Scheme 4. Probable Structures of $[9MG{\cdot}1MC]^{\bullet+}{\cdot}H_2O$ Calculated at ωB97XD/6-311++G(d,p)

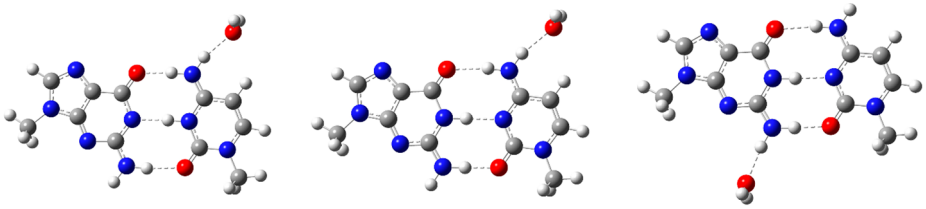

those for $9MG^{\bullet+} + {}^1O_2$. In each frame of Figure 1, pathways of the same type in $[9MG - H]^{\bullet} + {}^1O_2$ and $9MG^{\bullet+} + {}^1O_2$ are plotted side by side in a similar color scheme, and the same set of nomenclatures was adopted for intermediates and TSs in the two systems. This allows easy comparison between the two systems. Despite the different charge states of $[9MG - H]^{\bullet}$ versus $9MG^{\bullet+}$, $[9MG - H]^{\bullet}$ essentially follows the same reaction coordinate and produces the same type of products as $9MG^{\bullet+}$ (also see the reaction structure of $[9MG - H]^{\bullet} + {}^1O_2$ in Scheme S1 in the Supporting Information). The major difference is the missing of a pathway leading from [5-OO-9MG − H]• to [5,8-OO-9MG − H]•, but this pathway is less likely to be important as there is a concerted pathway leading to 5,8-addition.

Compared to those of $9MG^{\bullet+}$, the C5- and C8-terminal additions and 5,8-cycloaddition of $[9MG - H]^{\bullet}$ become more energetically favorable as the corresponding TSs and products decrease in energy by 0.1−0.3 eV. The only exception is the C4-addition, for which the energies of TS4 and [4-OO-9MG − H]• increase by 0.2 eV than those of $9MG^{\bullet+}$. However, the C4-addition does not represent a favorable pathway in either system. It can therefore be concluded that $[9MG - H]^{\bullet}$ should possess the same reactivity toward $^1O_2$ as, if not higher than, $9MG^{\bullet+}$.

Again, the spin-projected ωB97XD and CASPT2(21,15) have predicted similar reaction energetics for most reaction structures of $[9MG - H]^{\bullet} + {}^1O_2$, whereas the DLPNO-CCSD(T) calculated energies are generally lower by more than 0.2 eV (see Table 2).

4.2. Reaction Products and Cross Sections of $[9MG{\cdot}1MC]^{\bullet+}$ with $^1O_2$. Similar to that in the $^1O_2$ reaction with dry $9MG^{\bullet+}$, products in the $^1O_2$ reaction with dry $[9MG{\cdot}1MC]^{\bullet+}$ were not directly detected with the mass spectrometer. This was again because any O_2-adducts forming in the reaction decomposed to starting reactants due to internal excitation gained from the reaction heat release, and product decomposition happened within the mass spectrometer time-of-flight. The CID of $[9MG{\cdot}1MC]^{\bullet+}$ by O_2 was observed at high energies,[28] but this is not of primary interest here and will not be discussed further. To capture transient oxidation products of the base pair, $[9MG{\cdot}1MC]^{\bullet+}{\cdot}H_2O$ was then used as the target reactant ion, as we did in the experiment of $9MG^{\bullet+}{\cdot}H_2O$ with $^1O_2$. Product ions of $[9MG{\cdot}1MC]^{\bullet+}{\cdot}H_2O$ (m/z 308) + $^1O_2$ were indeed observed at m/z 322, which corresponds to the liberation of a water ligand from the adduct $[9MG{\cdot}1MC\text{-}O_2]^{\bullet+}{\cdot}H_2O$. Figure 2a shows a representative product ion mass spectrum. No oxidation product ions were observed in the collisions of $^1O_2$ with monomeric $[1MC + H]^+$ or $[1MC + H]^+{\cdot}H_2O$, which rules out the reactivity of the cytosine moiety toward $^1O_2$. Neither was a $9MG^{\bullet+}\text{-}O_2$ or a $[9MG^{\bullet+}\text{-}O_2]{\cdot}H_2O$ adduct detected, indicating that the $^1O_2$ oxidation did not lead to base pair dissociation.

Reaction cross reaction and efficiency for $[9MG{\cdot}1MC]^{\bullet+}{\cdot}H_2O + {}^1O_2$ are shown in Figure 2b as a function of collision energy in the center-of-mass frame. The efficiency was measured to be 1.2% at E_{col} = 0.05 eV, 0.8% at 0.1 eV, and less than 0.1% at energies above 0.2 eV. Uncertainties in the cross sections were determined from four sets of measurements. The energy-dependent $^1O_2$ oxidation behavior of $[9MG{\cdot}1MC]^{\bullet+}$ closely matches that of the monomeric $9MG^{\bullet+}$. The reaction efficiency of $[9MG{\cdot}1MC]^{\bullet+}$ is strongly suppressed by collision energy, and it decreases even faster at high energies than that of $9MG^{\bullet+}$. The strong suppression is again attributed to the reduced complex intermediacy at high energies.

$[9MG{\cdot}1MC]^{\bullet+}{\cdot}H_2O$ has multiple conformers because of various water-binding motifs and intra-base pair PT.[28] The three lowest-energy conformers are provided in Scheme 4, with their Cartesian coordinates reported in the Supporting Information. The hydration energy of $[9MG{\cdot}1MC]^{\bullet+}{\cdot}H_2O$ ($\Delta H_{hydration} = \Delta H_{monohydrate} - \Delta H_{dry\ ion} - \Delta H_{water}$) arises largely from a charge−dipole interaction, and the interaction energy of the water ligand with the 9MG moiety is comparable to that with the 1MC moiety. Based on the ωB97XD/6-311++G(d,p) calculations, $\Delta H_{hydration}$ of the most important conformer (population = 55%) is 0.48 eV, that for the second important conformer (population = 22%) is 0.41 eV, and that for the third important

https://doi.org/10.1021/acs.jpcb.2c03748
J. Phys. Chem. B 2022, 126, 5458−5472

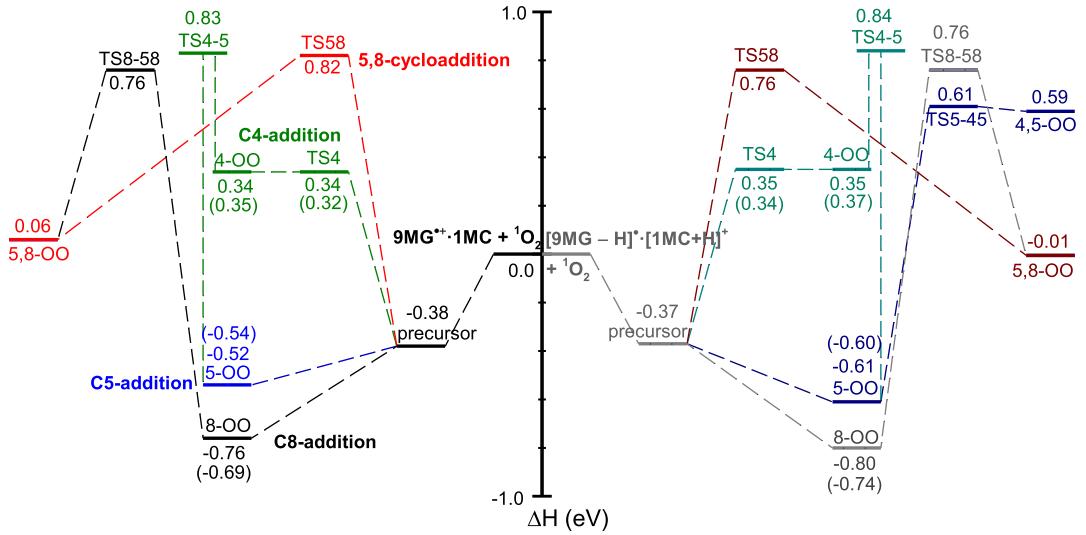

Figure 3. Reaction PES for (left) $9MG^{\bullet+}$·1MC + $^1O_2$ and (right) $[9MG - H]^{\bullet}$·$[1MC + H]^+$ + $^1O_2$, calculated at spin-projected ωB97XD/6-31+G(d,p). For 4-, 5-, and 8-peroxides and corresponding TSs, enthalpies for both *syn*- and *anti*-conformers are provided, with the *anti* listed in parentheses.

one (population = 15%) is 0.40 eV. We have also identified a PT structure of the third conformer, but it has an insignificant population and is thus ignored. The sum of three conformers accounts for 92% of the monohydrated reactant ions in the experiment. It implies that the formation exothermicity of the product ions which were detected in the experiment should be at least no less than 0.4 eV, as only in this case was the reaction system capable of eliminating the water ligand barrierlessly upon O_2-addition. The present result has thus provided a benchmark thermodynamic measurement, which will be used in the next section to determine the reliability of PES calculations.

4.3. Reaction PES for $[9MG{\cdot}1MC]^{\bullet+}$ with $^1O_2$. The comparison of single nucleobase reaction PESs calculated at different levels of theory has verified that the spin-projected ωB97XD and CASPT2(21,15) are able to reach consistent reaction energetics but not the DLPNO-CCSD(T). As the increasing number of molecular orbitals in $[9MG{\cdot}1MC]^{\bullet+}$ has made it difficult to choose/swap active orbitals in CASPT2 calculations, the spin-projected ωB97XD was used as a cost-effective yet reliable approach for constructing base pair PESs. DLPNO-CCSD(T) was used mainly for the T1 diagnostic.

Reaction PESs constructed at spin-projected ωB97XD are shown in Figure 3. Reaction energies, $\langle \hat{S}^2 \rangle$, and T1 diagnostic results for the $9MG^{\bullet+}$·1MC and $[9MG - H]^{\bullet}$·$[1MC + H]^+$ systems are appended to Tables 1 and 2 (in gray shaded cells), so that a direct comparison could be made with their single nucleobase analogues. Similar to what was seen in the reactions of single nucleobases, the DLPNO-CCSD(T) energies for base pair reaction structures are −0.18 to −0.49 eV lower than their spin-projected ωB97XD energies due to the aforementioned deficiency in the CCSD(T) calculations.

Comparison of the $^1O_2$ oxidation of monomeric guanine radicals versus those within a base pair aids our understanding of how structural context influences DNA oxidative damage. Consequences on reaction pathways are revealed as follows:

(1) **Effect of intra-base pair PT**: $9MG^{\bullet+}$·1MC and $[9MG - H]^{\bullet}$·$[1MC + H]^+$ follow essentially the same reaction pathways, except for the lack of a 4,5-addition pathway in $9MG^{\bullet+}$·1MC. The formation of an 8-peroxide represents the most probable product channel with no barriers above the reactants, followed by a 5-peroxide. On the other hand, 5,8-cycloaddition and C4-addition are both endothermic and have been ruled out by the experiment.

(2) **Effect of base pairing**: $9MG^{\bullet+}$·1MC presents a reactivity toward $^1O_2$ similar to that of the $9MG^{\bullet+}$ monomer. The differences are the lack of a stepwise 4,5-addition leading from $[4\text{-OO-9MG}]^{\bullet+}$·1MC and a stepwise 5,8-addition leading from $[5\text{-OO-9MG}]^{\bullet+}$·1MC. Similarly, $[9MG - H]^{\bullet}$·$[1MC + H]^+$ presents the same types of $^1O_2$ reactions as those occur to the $[9MG - H]^{\bullet}$ monomer.

(3) **Electrostatic effect**: for both monomeric nucleobases and those within a base pair, the neutral guanine radical presents up to 0.3 eV favorability for C5-addition, C8-addition, 5,8-cycloaddition, and 4,5-addition. This is because a neutral $[9MG - H]^{\bullet}$ moiety is more favored by electrophilic $^1O_2$ attack.

(4) **Effect on reaction energetics**: singlet oxygenation renders the proton-transferred base pair structure more stable than the conventional structure. $[9MG - H]^{\bullet}$·$[1MC + H]^+$ is 0.05 eV higher in energy than $9MG^{\bullet+}$·1MC, but the peroxide products of $[9MG - H]^{\bullet}$·$[1MC + H]^+$ (except 4-peroxide) either present the same energy as or become more stable than the corresponding products of $9MG^{\bullet+}$·1MC. The implication is that an oxidized base pair becomes in favor of a proton-transferred structure.

(5) **Effect on base pair strength**: singlet oxygenation slightly increases base pairing energy in a conventional structure, whereas it significantly decreases base pairing energy in a proton-transferred structure. The complexation energy (with BSSE corrections) is 2.24 eV for $9MG^{\bullet+}$·1MC versus 2.20 eV for $[9MG - H]^{\bullet}$·$[1MC + H]^+$; after O_2 addition, it becomes 2.26 eV for *syn*-/*anti*-$8\text{-OO-9MG}^{\bullet+}$·1MC versus 2.01−2.05 eV for *syn*-/*anti*-$[8\text{-OO-9MG} - H]^{\bullet}$·$[1MC + H]^+$. Similarly, the complexation energy is 2.30 eV for *syn*-/*anti*-$5\text{-OO-9MG}^{\bullet+}$·1MC versus 2.01−2.06 eV for *syn*-/*anti*-$[8\text{-OO-9MG} - H]^{\bullet}$·$[1MC + H]^+$.

https://doi.org/10.1021/acs.jpcb.2c03748
J. Phys. Chem. B 2022, 126, 5458−5472

5. COMPARISON WITH PREVIOUS SYSTEMS AND BIOLOGICAL IMPLICATIONS

The experimental and computational studies of the $^1O_2$ reaction with deprotonated guanine−cytosine ($[G{\cdot}C - H]^-$) were reported by our laboratory.[66] A unsubstituted guanine possess two tautomeric structures: 9H-guanine (9HG) with H atoms positioned at N1 and N9 and 7H-guanine (7HG) with H atoms at N1 and N7;[64] therefore, the base pair system consists of 9HG·$[G - H_{N1'}]^-$ and 7HG·$[C - H_{N1'}]^-$ as well as their PT conformers $[9HG - H_{N1}]^-{\cdot}[C - H_{N1'} + H_{N3'}]$ and $[7HG - H_{N1}]^-{\cdot}[C - H_{N1'} + H_{N3'}]$. As a consequence, $^1O_2$ oxidation gets entangled with guanine tautomerization and intra-base pair PT. Using $[G{\cdot}C - H]^-{\cdot}H_2O$ as the reactant ion, the conformer-averaged reaction cross section was measured to be 0.75 Å^2 at E_{col} = 0.1 eV (corresponding to a reaction efficiency of 1.1%). Accordingly, the reactivity of $[G{\cdot}C - H]^-$ appears to be comparable with that of $[9MG{\cdot}1MC]^{\bullet+}$ (0.8%) at the same energy.

The major differences between the base pair radical cation and its deprotonated counterpart are reaction pathways and product structures. Direct dynamics trajectory simulations were used to mimic tautomer-specific reactions of $[G{\cdot}C - H]^-$ under experimental conditions. It was found that the 9HG-containing $[G{\cdot}C - H]^-$ favors stepwise formation of a 4,8-endoperoxide of guanine, while the 7HG-containing $[G{\cdot}C - H]^-$ prefers a concerted formation of a 5,8-endoperoxide of guanine. Neither of the two product channels appears in the reaction of $[9MG{\cdot}1MC]^{\bullet+}$. The only common feature for $[9MG{\cdot}1MC]^{\bullet+}$ and $[G{\cdot}C - H]^-$ is that the PT conformers have lower activation barriers for $^1O_2$ addition than their conventional conformers.

A variety of oxidation behaviors were also reported for singlet oxygenation of neutral guanosine (forms a 4,8-endoperoxide via a concerted cycloaddition),[48] $[9HG + H]^+$ (forms a 5,8-endoperoxide via a concerted cycloaddition),[64] $[9HG - H]^-$ (forms a 5,8-endoperoxide via a concerted cycloaddition),[64] $9MG^{\bullet+}$ (forms an 8-peroxide),[41] $[9MG + H]^+$ (forms a 5,8-endoperoxide via a concerted cycloaddition),[65] and $[9MG - H]^-$ (stepwise addition starting with the formation of an 8-peroxide and subsequently evolving to a 4,8-endoperoxide).[65] These findings demonstrate the interplay between guanine structure and oxidizability. Guanine ionization, tautomerization, N9-substitution, and intra-base pair PT are all crucial in determining oxidation mechanisms, dynamics, kinetics, and products.

6. CONCLUSIONS

The present work has assessed the chemistry of $^1O_2$ with a 9MG nucleobase in a radical cation versus a dehydrogenated neutral radical and either as an isolated monomer or paired with a complementary cytosine within a Watson−Crick base pair. The guided-ion beam experimental findings were rationalized in light of theoretical modeling using the approximately spin-projected ωB97XD/6-31+G(d,p), DLPNO-CCSD(T)/aug-cc-pVQZ, and multireferential CASPT2(21,15)/6-31G(d,p) methods. The combined experimental and theoretical work reveal the following points: (i) initial $^1O_2$ addition to guanine radicals in different structural contexts all leads to an 8-peroxide structure. The reaction is exothermic with no activation barriers above the starting reactants. The product exothermicity is high enough to liberate a water ligand bound to the reaction system; (ii) the distinctively different $^1O_2$ reaction pathways of the guanine radical cation than those of a neutral guanine molecule and protonated/deprotonated guanine ions emphasize the strong dependence of the nucleobase oxidation mechanism on the ionization states; (iii) intra-base pair PT enhances the oxidization efficiency by lowering the reaction activation barriers and/or stabilizing products; (iv) other probable reaction routes include a concerted 5,8-cycloaddition to the formation of an endoperoxide $[5,8\text{-OO-9MG}]^{\bullet+}$ and C4- and C5-terminal addition pathways to the formation of a $[4\text{-OO-9MG}]^{\bullet+}$ and a $[5\text{-OO-9MG}]^{\bullet+}$ and then to a dioxetane $[4,5\text{-OO-9MG}]^{\bullet+}$.

■ ASSOCIATED CONTENT

Supporting Information

The Supporting Information is available free of charge at https://pubs.acs.org/doi/10.1021/acs.jpcb.2c03748.

Reaction structures for singlet oxygenation of $[9MG - H]^{\bullet}{\cdot}[1MC + H]^+$ and Cartesian coordinates for the calculated structures (PDF)

■ AUTHOR INFORMATION

Corresponding Author

Jianbo Liu − *Department of Chemistry and Biochemistry, Queens College of the City University of New York, Queens, New York 11367, United States; Ph.D. Program in Chemistry, The Graduate Center of the City University of New York, New York, New York 10016, United States;* orcid.org/0000-0001-9577-3740; Phone: 1-718-997-3271; Email: jianbo.liu@qc.cuny.edu

Authors

May Myat Moe − *Department of Chemistry and Biochemistry, Queens College of the City University of New York, Queens, New York 11367, United States; Ph.D. Program in Chemistry, The Graduate Center of the City University of New York, New York, New York 10016, United States;* orcid.org/0000-0001-9444-2982

Toru Saito − *Department of Biomedical Information Science, Graduate School of Information Science, Hiroshima City University, 731-3194 Hiroshima, Japan;* orcid.org/0000-0002-8388-4555

Midas Tsai − *Department of Natural Sciences, LaGuardia Community College, Long Island City, New York 11101, United States*

Complete contact information is available at: https://pubs.acs.org/10.1021/acs.jpcb.2c03748

Notes

The authors declare no competing financial interest.

■ ACKNOWLEDGMENTS

This work was supported by the National Science Foundation (grant no. CHE 1856362). We thank Shuai Ma for assistance with the ChemDraw schematics.

■ REFERENCES

(1) Steenken, S.; Jovanovic, S. V. How Easily Oxidizable Is DNA? One-Electron Reduction Potentials of Adenosine and Guanosine Radicals in Aqueous Solution. *J. Am. Chem. Soc.* **1997**, *119*, 617−618.

(2) Burrows, C. J.; Muller, J. G. Oxidative Nucleobase Modifications Leading to Strand Scission. *Chem. Rev.* **1998**, *98*, 1109−1152.

(3) Zhou, J.; Kostko, O.; Nicolas, C.; Tang, X.; Belau, L.; de Vries, M. S.; Ahmed, M. Experimental Observation of Guanine Tautomers with VUV Photoionization. *J. Phys. Chem. A* **2009**, *113*, 4829−4832.

(4) Schwell, M.; Hochlaf, M. Photoionization Spectroscopy of Nucleobases and Analogues in the Gas Phase Using Synchrotron Radiation as Excitation Light Source. *Top. Curr. Chem.* **2015**, *355*, 155−208.
(5) Candeias, L. P.; Steenken, S. Ionization of Purine Nucleosides and Nucleotides and Their Components by 193-nm Laser Photolysis in Aqueous Solution: Model Studies for Oxidative Damage of DNA. *J. Am. Chem. Soc.* **1992**, *114*, 699−704.
(6) Pluhařová, E.; Oncak, M.; Seidel, R.; Schroeder, C.; Schroeder, W.; Winter, B.; Bradforth, S. E.; Jungwirth, P.; Slavicek, P. Transforming Anion Instability into Stability: Contrasting Photoionization of Three Protonation Forms of the Phosphate Ion Upon Moving into Water. *J. Phys. Chem. B* **2012**, *116*, 13254−13264.
(7) Schroeder, C. A.; Pluhařová, E.; Seidel, R.; Schroeder, W. P.; Faubel, M.; Slavíček, P.; Winter, B.; Jungwirth, P.; Bradforth, S. E. Oxidation Half-Reaction of Aqueous Nucleosides and Nucleotides via Photoelectron Spectroscopy Augmented by Ab Initio Calculations. *J. Am. Chem. Soc.* **2015**, *137*, 201−209.
(8) Crespo-Hernández, C. E.; Arce, R.; Ishikawa, Y.; Gorb, L.; Leszczynski, J.; Close, D. M. Ab Initio Ionization Energy Thresholds of DNA and RNA Bases in Gas Phase and in Aqueous Solution. *J. Phys. Chem. A* **2004**, *108*, 6373−6377.
(9) Fernando, H.; Papadantonakis, G. A.; Kim, N. S.; LeBreton, P. R. Conduction-Band-Edge Ionization Thresholds of DNA Components in Aqueous Solution. *Proc. Natl. Acad. Sci. U.S.A.* **1998**, *95*, 5550−5555.
(10) Caruso, T.; Carotenuto, M.; Vasca, E.; Peluso, A. Direct Experimental Observation of the Effect of the Base Pairing on the Oxidation Potential of Guanine. *J. Am. Chem. Soc.* **2005**, *127*, 15040−15041.
(11) Crespo-Hernandez, C. E.; Close, D. M.; Gorb, L.; Leszczynski, J. Determination of Redox Potentials for the Watson-Crick Base Pairs, DNA Nucleosides, and Relevant Nucleoside Analogs. *J. Phys. Chem. B* **2007**, *111*, 5386−5395.
(12) Hutter, M.; Clark, T. On the Enhanced Stability of the Guanine-Cytosine Base-Pair Radical Cation. *J. Am. Chem. Soc.* **1996**, *118*, 7574−7577.
(13) Jaeger, H. M.; Schaefer, H. F., III. Characterizing Radiation-Induced Oxidation of DNA by Way of the Monohydrated Guanine-Cytosine Radical Cation. *J. Phys. Chem. B* **2009**, *113*, 8142−8148.
(14) Nikogosyan, D. N. Two-Quantum Uv Photochemistry of Nucleic Acids: Comparison with Conventional Low-Intensity UV Photochemistry and Radiation Chemistry. *Int. J. Radiat. Biol.* **1990**, *57*, 233−299.
(15) Candeias, L. P.; Steenken, S. Structure and Acid-Base Properties of One-Electron-Oxidized Deoxyguanosine, Guanosine, and 1-Methylguanosine. *J. Am. Chem. Soc.* **1989**, *111*, 1094−1099.
(16) Steenken, S. Purine Bases, Nucleosides, and Nucleotides: Aqueous Solution Redox Chemistry and Transformation Reactions of Their Radical Cations and e^- and OH Adducts. *Chem. Rev.* **1989**, *89*, 503−520.
(17) Saito, I.; Nakamura, T.; Nakatani, K. Mapping of Highest Occupied Molecular Orbitals of Duplex DNA by Cobalt-Mediated Guanine Oxidation. *J. Am. Chem. Soc.* **2000**, *122*, 3001−3006.
(18) Stemp, E. D.; Barton, J. K. Electron Transfer between Metal Complexes Bound to DNA: Is DNA a Wire? *Met. Ions Biol. Syst.* **1996**, *33*, 325−365.
(19) Thorp, H. H. Cutting out the Middleman: DNA Biosensors Based on Electrochemical Oxidation. *Trends Biotechnol.* **1998**, *16*, 117−121.
(20) Kasai, H.; Yamaizumi, Z.; Berger, M.; Cadet, J. Photosensitized Formation of 7,8-Dihydro-8-Oxo-2'-Deoxyguanosine (8-Hydroxy-2'-Deoxyguanosine) in DNA by Riboflavin: A Non Singlet Oxygen-Mediated Reaction. *J. Am. Chem. Soc.* **1992**, *114*, 9692−9694.
(21) Lewis, F. D.; Liu, X.; Liu, J.; Miller, S. E.; Hayes, R. T.; Wasielewski, M. R. Direct Measurement of Hole Transport Dynamics in DNA. *Nature* **2000**, *406*, 51−53.
(22) Kobayashi, K.; Tagawa, S. Direct Observation of Guanine Radical Cation Deprotonation in Duplex DNA Using Pulse Radiolysis. *J. Am. Chem. Soc.* **2003**, *125*, 10213−10218.
(23) Kobayashi, K.; Yamagami, R.; Tagawa, S. Effect of Base Sequence and Deprotonation of Guanine Cation Radical in DNA. *J. Phys. Chem. B* **2008**, *112*, 10752−10757.
(24) Dean, J. A. *Lange's Handbook of Chemistry*; McGraw-Hill: New York, 1999.
(25) Parker, A. W.; Lin, C. Y.; George, M. W.; Towrie, M.; Kuimova, M. K. Infrared Characterization of the Guanine Radical Cation: Finger Printing DNA Damage. *J. Phys. Chem. B* **2010**, *114*, 3660−3667.
(26) Rokhlenko, Y.; Cadet, J.; Geacintov, N. E.; Shafirovich, V. Mechanistic Aspects of Hydration of Guanine Radical Cations in DNA. *J. Am. Chem. Soc.* **2014**, *136*, 5956−5962.
(27) Feketeová, L.; Chan, B.; Khairallah, G. N.; Steinmetz, V.; Maitre, P.; Radom, L.; O'Hair, R. A. J. Watson−Crick Base Pair Radical Cation as a Model for Oxidative Damage in DNA. *J. Phys. Chem. Lett.* **2017**, *8*, 3159−3165.
(28) Sun, Y.; Moe, M. M.; Liu, J. Mass Spectrometry and Computational Study of Collision-Induced Dissociation of 9-Methylguanine-1-Methylcytosine Base-Pair Radical Cation: Intra-Base-Pair Proton Transfer and Hydrogen Transfer, Non-Statistical Dissociation, and Reaction with a Water Ligand. *Phys. Chem. Chem. Phys.* **2020**, *22*, 14875−14888.
(29) Löwdin, P. O. Proton Tunneling in DNA [Deoxyribonucleic Acid] and Its Biological Implications. *Rev. Mod. Phys.* **1963**, *35*, 724−732. discussion 732-723
(30) Fu, L.-Y.; Wang, G.-Z.; Ma, B.-G.; Zhang, H.-Y. Exploring the Common Molecular Basis for the Universal DNA Mutation Bias: Revival of Löwdin Mutation Model. *Biochem. Biophys. Res. Commun.* **2011**, *409*, 367−371.
(31) Shukla, L. I.; Adhikary, A.; Pazdro, R.; Becker, D.; Sevilla, M. D. Formation of 8-Oxo-7,8-Dihydroguanine-Radicals in γ-Irradiated DNA by Multiple One-Electron Oxidations. *Nucleic Acids Res.* **2004**, *32*, 6565−6574.
(32) Wetmore, S. D.; Boyd, R. J.; Eriksson, L. A. Comparison of Experimental and Calculated Hyperfine Coupling Constants. Which Radicals Are Formed in Irradiated Guanine? *J. Phys. Chem. B* **1998**, *102*, 9332−9343.
(33) Sun, Y.; Zhou, W.; Moe, M. M.; Liu, J. Reactions of Water with Radical Cations of Guanine, 9-Methylguanine, 2'-Deoxyguanosine and Guanosine: Keto-Enol Isomerization, C8-Hydroxylation, and Effects of N9-Substitution. *Phys. Chem. Chem. Phys.* **2018**, *20*, 27510−27522.
(34) Zhou, W.; Liu, J. Reaction Mechanism and Dynamics for C8-Hydroxylation of 9-Methylguanine Radical Cation by Water Molecules. *Phys. Chem. Chem. Phys.* **2021**, *23*, 24464−24477.
(35) Cadet, J.; Douki, T.; Ravanat, J.-L. Oxidatively Generated Damage to the Guanine Moiety of DNA: Mechanistic Aspects and Formation in Cells. *Acc. Chem. Res.* **2008**, *41*, 1075−1083.
(36) Candeias, L. P.; Steenken, S. Reaction of $HO^•$ with Guanine Derivatives in Aqueous Solution: Formation of Two Different Redox-Active OH-Adduct Radicals and Their Unimolecular Transformation Reactions. Properties of G(-H)$^•$. *Chem.—Eur. J.* **2000**, *6*, 475−484.
(37) Reynisson, J.; Steenken, S. DFT Calculations on the Electrophilic Reaction with Water of the Guanine and Adenine Radical Cations. A Model for the Situation in DNA. *Phys. Chem. Chem. Phys.* **2002**, *4*, 527−532.
(38) Douki, T.; Spinelli, S.; Ravanat, J.-L.; Cadet, J. Hydroxyl Radical-Induced Degradation of 2'-Deoxyguanosine under Reducing Conditions. *J. Chem. Soc., Perkin Trans. 2* **1999**, 1875−1880.
(39) Alshykhly, O. R.; Fleming, A. M.; Burrows, C. J. 5-Carboxamido-5-Formamido-2-Iminohydantoin, in Addition to 8-Oxo-7,8-Dihydroguanine, Is the Major Product of the Iron-Fenton or X-Ray Radiation-Induced Oxidation of Guanine under Aerobic Reducing Conditions in Nucleoside and DNA Contexts. *J. Org. Chem.* **2015**, *80*, 6996−7007.
(40) Cadet, J.; Berger, M.; Buchko, G. W.; Joshi, P. C.; Raoul, S.; Ravanat, J.-L. 2,2-Diamino-4-[(3,5-Di-O-Acetyl-2-Deoxy-B-D-Erythro-Pentofuranosyl)Amino]-5-(2h)-Oxazolone: A Novel and Predominant Radical Oxidation Product of 3',5'-Di-O-Acetyl-2'-Deoxyguanosine. *J. Am. Chem. Soc.* **1994**, *116*, 7403−7404.
(41) Sun, Y.; Tsai, M.; Moe, M. M.; Liu, J. Dynamics and Multiconfiguration Potential Energy Surface for the Singlet O2

https://doi.org/10.1021/acs.jpcb.2c03748
J. Phys. Chem. B 2022, 126, 5458−5472

Reactions with Radical Cations of Guanine, 9-Methylguanine, 2′-Deoxyguanosine, and Guanosine. *J. Phys. Chem. A* **2021**, *125*, 1564−1576.
(42) Ogilby, P. R. Singlet Oxygen: There Is Indeed Something New under the Sun. *Chem. Soc. Rev.* **2010**, *39*, 3181−3209.
(43) Nonell, S.; Flors, C. *Singlet Oxygen: Applications in Biosciences and Nanosciences*; RSC: Cambridge, 2016; Vol. *1*, p 472.
(44) Ravanat, J.-L.; Di Mascio, P.; Martinez, G. R.; Medeiros, M. H. G.; Cadet, J. Singlet Oxygen Induces Oxidation of Cellular DNA. *J. Biol. Chem.* **2000**, *275*, 40601−40604.
(45) Cadet, J.; Douki, T.; Pouget, J.-P.; Ravanat, J.-L. Singlet Oxygen DNA Damage Products: Formation and Measurement. *Methods Enzymol.* **2000**, *319*, 143−153.
(46) Cadet, J.; Ravanat, J.-L.; Martinez, G. R.; Medeiros, M. H. G.; Di Mascio, P. Singlet Oxygen Oxidation of Isolated and Cellular DNA: Product Formation and Mechanistic Insights. *Photochem. Photobiol.* **2006**, *82*, 1219−1225.
(47) Cadet, J.; Douki, T.; Ravanat, J.-L. Oxidatively Generated Base Damage to Cellular DNA. *Free Radic. Biol. Med.* **2010**, *49*, 9−21.
(48) Sheu, C.; Foote, C. S. Endoperoxide Formation in a Guanosine Derivative. *J. Am. Chem. Soc.* **1993**, *115*, 10446−10447.
(49) Ravanat, J.-L.; Douki, T.; Cadet, J. Direct and Indirect Effects of UV Radiation on DNA and Its Components. *J. Photochem. Photobiol., B* **2001**, *63*, 88−102.
(50) Ravanat, J.-L.; Saint-Pierre, C.; Di Mascio, P.; Martinez, G. R.; Medeiros, M. H. G.; Cadet, J. Damage to Isolated DNA Mediated by Singlet Oxygen. *Helv. Chim. Acta* **2001**, *84*, 3702−3709.
(51) Niles, J. C.; Wishnok, J. S.; Tannenbaum, S. R. Spiroiminodihydantoin Is the Major Product of the 8-Oxo-7,8-Dihydroguanosine Reaction with Peroxynitrite in the Presence of Thiols and Guanosine Photooxidation by Methylene Blue. *Org. Lett.* **2001**, *3*, 963−966.
(52) Kang, P.; Foote, C. S. Formation of Transient Intermediates in Low-Temperature Photosensitized Oxidation of an 8-13c-Guanosine Derivative. *J. Am. Chem. Soc.* **2002**, *124*, 4865−4873.
(53) Ye, Y.; Muller, J. G.; Luo, W.; Mayne, C. L.; Shallop, A. J.; Jones, R. A.; Burrows, C. J. Formation of ^{13}C-, ^{15}N-, and ^{18}O-Labeled Guanidinohydantoin from Guanosine Oxidation with Singlet Oxygen. Implications for Structure and Mechanism. *J. Am. Chem. Soc.* **2003**, *125*, 13926−13927.
(54) Ravanat, J.-L.; Martinez, G. R.; Medeiros, M. H. G.; Di Mascio, P.; Cadet, J. Mechanistic Aspects of the Oxidation of DNA Constituents Mediated by Singlet Molecular Oxygen. *Arch. Biochem. Biophys.* **2004**, *423*, 23−30.
(55) McCallum, J. E. B.; Kuniyoshi, C. Y.; Foote, C. S. Characterization of 5-Hydroxy-8-Oxo-7,8-Dihydroguanosine in the Photosensitized Oxidation of 8-Oxo-7,8-Dihydroguanosine and Its Rearrangement to Spiroiminodihydantoin. *J. Am. Chem. Soc.* **2004**, *126*, 16777−16782.
(56) Iesce, M.; Cermola, F.; Temussi, F. Photooxygenation of Heterocycles. *Curr. Org. Chem.* **2005**, *9*, 109−139.
(57) Neeley, W. L.; Essigmann, J. M. Mechanisms of Formation, Genotoxicity, and Mutation of Guanine Oxidation Products. *Chem. Res. Toxicol.* **2006**, *19*, 491−505.
(58) Ravanat, J.-L.; Martinez, G. R.; Medeiros, M. H. G.; Di Mascio, P.; Cadet, J. Singlet Oxygen Oxidation of 2'-Deoxyguanosine. Formation and Mechanistic Insights. *Tetrahedron* **2006**, *62*, 10709−10715.
(59) Gimisis, T.; Cismaş, C. Isolation, Characterization, and Independent Synthesis of Guanine Oxidation Products. *Eur. J. Org. Chem.* **2006**, *2006*, 1351−1378.
(60) Dumont, E.; Gruber, R.; Grüber, E.; Morell, C.; Moreau, Y.; Monari, A.; Ravanat, J.-L. Probing the Reactivity of Singlet Oxygen with Purines. *Nucleic Acids Res.* **2016**, *44*, 56−62.
(61) Dumont, E.; Gruber, R.; Grüber, E.; Morell, C.; Aranda, J.; Ravanat, J.-L.; Tuñón, I. Singlet Oxygen Attack on Guanine: Reactivity and Structural Signature within the B-DNA Helix. *Chem.—Eur. J.* **2016**, *22*, 12358−12362.
(62) Fleming, A. M.; Burrows, C. J. Formation and Processing of DNA Damage Substrates for the hNEIL Enzymes. *Free Radic. Biol. Med.* **2017**, *107*, 35−52.
(63) Thapa, B.; Munk, B. H.; Burrows, C. J.; Schlegel, H. B. Computational Study of Oxidation of Guanine by Singlet Oxygen ($^1\Delta_g$) and Formation of Guanine:Lysine Cross-Links. *Chem.—Eur. J.* **2017**, *23*, 5804−5813.
(64) Lu, W.; Liu, J. Capturing Transient Endoperoxide in the Singlet Oxygen Oxidation of Guanine. *Chem.—Eur. J.* **2016**, *22*, 3127−3138.
(65) Lu, W.; Teng, H.; Liu, J. How Protonation and Deprotonation of 9-Methylguanine Alter Its Singlet O_2 Addition Path: About the Initial Stage of Guanine Nucleoside Oxidation. *Phys. Chem. Chem. Phys.* **2016**, *18*, 15223−15234.
(66) Lu, W.; Sun, Y.; Tsai, M.; Zhou, W.; Liu, J. Singlet O_2 Oxidation of Deprotonated Guanine-Cytosine Base Pair and Its Entangling with Intra-Base-Pair Proton Transfer. *ChemPhysChem* **2018**, *19*, 2645−2654.
(67) Lu, W.; Sun, Y.; Zhou, W.; Liu, J. Ph-Dependent Singlet O_2 Oxidation Kinetics of Guanine and 9-Methylguanine: An Online Mass Spectrometry and Spectroscopy Study Combined with Theoretical Exploration. *J. Phys. Chem. B* **2018**, *122*, 40−53.
(68) Sun, Y.; Tsai, M.; Zhou, W.; Lu, W.; Liu, J. Reaction Kinetics, Product Branching, and Potential Energy Surfaces of $^1O_2$-Induced 9-Methylguanine−Lysine Cross-Linking: A Combined Mass Spectrometry, Spectroscopy, and Computational Study. *J. Phys. Chem. B* **2019**, *123*, 10410−10423.
(69) Colasanti, A.; Kisslinger, A.; Quarto, M.; Riccio, P. Combined Effects of Radiotherapy and Photodynamic Therapy on an *in Vitro* Human Prostate Model. *Acta Biochim. Pol.* **2004**, *51*, 1039−1046.
(70) Postiglione, I.; Chiaviello, A.; Palumbo, G. Enhancing Photodynamic Therapy Efficacy by Combination Therapy: Dated, Current and Oncoming Strategies. *Cancers* **2011**, *3*, 2597−2629.
(71) Lo, V. C. K.; Akens, M. K.; Moore, S.; Yee, A. J. M.; Wilson, B. C.; Whyne, C. M. Beyond Radiation Therapy: Photodynamic Therapy Maintains Structural Integrity of Irradiated Healthy and Metastatically Involved Vertebrae in a Pre-Clinical *in Vivo* Model. *Breast Cancer Res. Treat.* **2012**, *135*, 391−401.
(72) Midey, A.; Dotan, I.; Viggiano, A. A. Temperature Dependences for the Reactions of O^- and O_2^- with $O_2(a^1\Delta_g)$ from 200 to 700 K. *J. Phys. Chem. A* **2008**, *112*, 3040−3045.
(73) Fang, Y.; Liu, F.; Bennett, A.; Ara, S.; Liu, J. Experimental and Trajectory Study on Reaction of Protonated Methionine with Electronically Excited Singlet Molecular Oxygen ($a^1\Delta_g$): Reaction Dynamics and Collision Energy Effects. *J. Phys. Chem. B* **2011**, *115*, 2671−2682.
(74) Liu, F.; Fang, Y.; Chen, Y.; Liu, J. Reactions of Deprotonated Tyrosine and Tryptophan with Electronically Excited Singlet Molecular Oxygen ($a^1\Delta_g$): A Guided-Ion-Beam Scattering, Statistical Modeling, and Trajectory Study. *J. Phys. Chem. B* **2012**, *116*, 6369−6379.
(75) Wee, S.; O'Hair, R. A. J.; McFadyen, W. D. Can Radical Cations of the Constituents of Nucleic Acids Be Formed in the Gas Phase Using Ternary Transition Metal Complexes? *Rapid Commun. Mass Spectrom.* **2005**, *19*, 1797−1805.
(76) Lam, A. K. Y.; Abrahams, B. F.; Grannas, M. J.; McFadyen, W. D.; O'Hair, R. A. J. Tuning the Gas Phase Redox Properties of Copper(II) Ternary Complexes of Terpyridines to Control the Formation of Nucleobase Radical Cations. *Dalton Trans.* **2006**, 5051−5061.
(77) Feketeová, L.; Yuriev, E.; Orbell, J. D.; Khairallah, G. N.; O'Hair, R. A. J. Gas-Phase Formation and Reactions of Radical Cations of Guanosine, Deoxyguanosine and Their Homodimers and Heterodimers. *Int. J. Mass Spectrom.* **2011**, *304*, 74−82.
(78) Cheng, P.; Bohme, D. K. Gas-Phase Formation of Radical Cations of Monomers and Dimers of Guanosine by Collision-Induced Dissociation of Cu(Ii)-Guanosine Complexes. *J. Phys. Chem. B* **2007**, *111*, 11075−11082.
(79) Moe, M. M.; Tsai, M.; Liu, J. Singlet Oxygen Oxidation of the Radical Cations of 8-Oxo-2′-Deoxyguanosine and Its 9-Methyl Analogue: Dynamics, Potential Energy Surface, and Products Mediated by C5-O_2-Addition. *ChemPlusChem* **2021**, *86*, 1243−1254.

https://doi.org/10.1021/acs.jpcb.2c03748
J. Phys. Chem. B 2022, 126, 5458−5472

(80) Benny, J.; Saito, T.; Moe, M. M.; Liu, J. Singlet O_2 Reactions with Radical Cations of 8-Bromoguanine and 8-Bromoguanosine: Guided-Ion Beam Mass Spectrometric Measurements and Theoretical Treatments. *J. Phys. Chem. A* **2022**, *126*, 68−79.
(81) Huang, S. R.; Tureček, F. Cation Radicals of Hachimoji Nucleobases. Canonical Purine and Noncanonical Pyrimidine Forms Generated in the Gas Phase and Characterized by UV-Vis Photodissociation Action Spectroscopy. *J. Phys. Chem. A* **2020**, *124*, 7101−7112.
(82) Huang, S. R.; Tureček, F. Cation Radicals of Hachimoji Nucleobases P and Z: Generation in the Gas Phase and Characterization by UV-Vis Photodissociation Action Spectroscopy and Theory. *J. Am. Soc. Mass Spectrom.* **2021**, *32*, 373−386.
(83) Fang, Y.; Liu, J. Reaction of Protonated Tyrosine with Electronically Excited Singlet Molecular Oxygen ($a^1\Delta_g$): An Experimental and Trajectory Study. *J. Phys. Chem. A* **2009**, *113*, 11250−11261.
(84) Ervin, K. M.; Armentrout, P. B. Translational Energy Dependence of $Ar^+ + XY \rightarrow ArX^+ + Y$ (XY = H_2, D_2, HD) from Thermal to 30 eV C.M. *J. Chem. Phys.* **1985**, *83*, 166−189.
(85) Armentrout, P. B. Mass Spectrometry - Not Just a Structural Tool: The Use of Guided Ion Beam Tandem Mass Spectrometry to Determine Thermochemistry. *J. Am. Soc. Mass Spectrom.* **2002**, *13*, 419−434.
(86) Al-Sheikhly, M. The Reactivity of Adenyl and Guanyl Radicals Towards Oxygen. *Radiat. Phys. Chem.* **1994**, *44*, 297−301.
(87) Kumar, A.; Sevilla, M. D. Proton Transfer Induced Somo-to-Homo Level Switching in One-Electron Oxidized A-T and G-C Base Pairs: A Density Functional Theory Study. *J. Phys. Chem. B* **2014**, *118*, 5453−5458.
(88) van Duijneveldt, F. B.; van Duijneveldt-van de Rijdt, J. G. C. M.; van Lenthe, J. H. State of the Art in Counterpoise Theory. *Chem. Rev.* **1994**, *94*, 1873−1885.
(89) Boys, S. F.; Bernardi, F. The Calculation of Small Molecular Interactions by the Differences of Separate Total Energies. Some Procedures with Reduced Errors. *Mol. Phys.* **1970**, *19*, 553−566.
(90) Simon, S.; Duran, M.; Dannenberg, J. J. How Does Basis Set Superposition Error Change the Potential Surfaces for Hydrogen-Bonded Dimers? *J. Chem. Phys.* **1996**, *105*, 11024−11031.
(91) Frisch, M. J.; Trucks, G. W.; Schlegel, H. B.; Scuseria, G. E.; Robb, M. A.; Cheeseman, J. R.; Scalmani, G.; Barone, V.; Petersson, G. A.; Nakatsuji, H.; et al. *Gaussian 16*, Rev. B.01; Gaussian, Inc: Wallingford, CT, 2016.
(92) Maranzana, A.; Ghigo, G.; Tonachini, G. Diradical and Peroxirane Pathways in the [Π2 + Π2] Cycloaddition Reactions of $^1\Delta_g$ Dioxygen with Ethene, Methyl Vinyl Ether, and Butadiene: A Density Functional and Multireference Perturbation Theory Study. *J. Am. Chem. Soc.* **2000**, *122*, 1414−1423.
(93) Saito, T.; Nishihara, S.; Kataoka, Y.; Nakanishi, Y.; Matsui, T.; Kitagawa, Y.; Kawakami, T.; Okumura, M.; Yamaguchi, K. Transition State Optimization Based on Approximate Spin-Projection (AP) Method. *Chem. Phys. Lett.* **2009**, *483*, 168−171.
(94) Saito, T.; Nishihara, S.; Kataoka, Y.; Nakanishi, Y.; Kitagawa, Y.; Kawakami, T.; Yamanaka, S.; Okumura, M.; Yamaguchi, K. Reinvestigation of the Reaction of Ethylene and Singlet Oxygen by the Approximate Spin Projection Method. Comparison with Multireference Coupled-Cluster Calculations. *J. Phys. Chem. A* **2010**, *114*, 7967−7974.
(95) Saito, T.; Takano, Y. Spin-Projected Qm/Mm Free Energy Simulations for Oxidation Reaction of Guanine in B−DNA by Singlet Oxygen. *ChemPhysChem* **2021**, *22*, 561−568.
(96) Yamaguchi, K.; Jensen, F.; Dorigo, A.; Houk, K. N. A Spin-Correction Procedure for Unrestricted Hartree-Fock and Moeller-Plesset Wave Functions for Singlet Diradicals and Polyradicals. *Chem. Phys. Lett.* **1988**, *149*, 537−542.
(97) Liakos, D. G.; Sparta, M.; Kesharwani, M. K.; Martin, J. M. L.; Neese, F. Exploring the Accuracy Limits of Local Pair Natural Orbital Coupled-Cluster Theory. *J. Chem. Theory Comput.* **2015**, *11*, 1525−1539.
(98) Woon, D. E.; Dunning, T. H., Jr. Gaussian Basis Sets for Use in Correlated Molecular Calculations. III. The Atoms Aluminum through Argon. *J. Chem. Phys.* **1993**, *98*, 1358−1371.
(99) Wilson, A. K.; van Mourik, T.; Dunning, T. H. Gaussian Basis Sets for Use in Correlated Molecular Calculations. VI. Sextuple Zeta Correlation Consistent Basis Sets for Boron through Neon. *J. Mol. Struct.: THEOCHEM* **1996**, *388*, 339−349.
(100) Lee, T. J.; Taylor, P. R. A Diagnostic for Determining the Quality of Single-Reference Electron Correlation Methods. *Int. J. Quantum Chem. Symp.* **1989**, *36*, 199−207.
(101) Jayatilaka, D.; Lee, T. J. Open-shell coupled-cluster theory. *J. Chem. Phys.* **1993**, *98*, 9734−9747.
(102) Raghavachari, K.; Trucks, G. W.; Pople, J. A.; Head-Gordon, M. A Fifth-Order Perturbation Comparison of Electron Correlation Theories. *Chem. Phys. Lett.* **1989**, *157*, 479−483.
(103) Neese, F. The Orca Program System. *Wiley Interdiscip. Rev.: Comput. Mol. Sci.* **2012**, *2*, 73−78.
(104) Andersson, K.; Malmqvist, P. Å.; Roos, B. O. Second-Order Perturbation Theory with a Complete Active Space Self-Consistent Field Reference Function. *J. Chem. Phys.* **1992**, *96*, 1218−1226.
(105) Abe, M.; Gopakmar, G.; Nakajima, T.; Hirao, K. Relativistic Multireference Perturbation Theory: Complete Active-Space Second-Order Perturbation Theory (CASPT2) with the Four-Component Dirac Hamiltonian. In *Radiation Induced Molecular Phenomena in Nucleic Acids*; Shukla, K., Leszczynski, J., Eds.; Springer: Netherlands, 2008; pp 157−177.
(106) Roos, B. O.; Taylor, P. R.; Sigbahn, P. E. M. A Complete Active Space Scf Method (CASSCF) Using a Density Matrix Formulated Super-Ci Approach. *Chem. Phys.* **1980**, *48*, 157−173.
(107) Fdez Galván, I.; Vacher, M.; Alavi, A.; Angeli, C.; Aquilante, F.; Autschbach, J.; Bao, J. J.; Bokarev, S. I.; Bogdanov, N. A.; Carlson, R. K.; et al. Openmolcas: From Source Code to Insight. *J. Chem. Theory Comput.* **2019**, *15*, 5925−5964.
(108) Aquilante, F.; Autschbach, J.; Baiardi, A.; Battaglia, S.; Borin, V. A.; Chibotaru, L. F.; Conti, I.; De Vico, L.; Delcey, M.; Fdez Galván, I.; et al. Modern Quantum Chemistry with [Open]Molcas. *J. Chem. Phys.* **2020**, *152*, 214117.
(109) Roca-Sanjuán, D.; Rubio, M.; Merchán, M.; Serrano-Andrés, L. Ab Initio Determination of the Ionization Potentials of DNA and RNA Nucleobases. *J. Chem. Phys.* **2006**, *125*, 084302.
(110) Alecu, I. M.; Zheng, J.; Zhao, Y.; Truhlar, D. G. Computational Thermochemistry: Scale Factor Databases and Scale Factors for Vibrational Frequencies Obtained from Electronic Model Chemistries. *J. Chem. Theory Comput.* **2010**, *6*, 2872−2887.
(111) Troe, J. Statistical Adiabatic Channel Model of Ion-Neutral Dipole Capture Rate Constants. *Chem. Phys. Lett.* **1985**, *122*, 425−430.
(112) Williams, I. H.; Williams, N. H. Advances in Physical Organic Chemistry. *Advances in Physical Organic Chemistry*; Elsevier: San Diego, 2016; Vol. *50*, p 282.

https://doi.org/10.1021/acs.jpcb.2c03748
J. Phys. Chem. B 2022, 126, 5458−5472